HIGHWAY RESEARCH RECORD

Number 282

Soil Theories:
Reinforced Earth,
Displacements,
Bearing, and Seepage

6 Reports

Subject Area

63 Mechanics (Earth Mass)

HIGHWAY RESEARCH BOARD

DIVISION OF ENGINEERING NATIONAL RESEARCH COUNCIL
NATIONAL ACADEMY OF SCIENCES—NATIONAL ACADEMY OF ENGINEERING

Washington, D. C., 1969

Publication 1659

Price: $2.20

Available from

Highway Research Board
National Academy of Sciences
2101 Constitution Avenue
Washington, D.C. 20418

Department of Soils, Geology and Foundations

Eldon J. Yoder, Chairman
Purdue University, Lafayette, Indiana

Chester McDowell, Vice Chairman
Texas Highway Department, Austin

HIGHWAY RESEARCH BOARD STAFF

J. W. Guinnee

Harry R. Cedergren
Robert C. Deen
Ernest Dobrovolny
W. B. Drake
Edwin B. Eckel
L. F. Erickson
Jacob Feld
Fred N. Finn
Charles R. Foster
LeRoy D. Graves
William B. Greene
William P. Hofmann
James M. Hoover
William S. Housel
Philip Keene
Miles S. Kersten
Delbert L. Lacey
T. William Lambe
G. A. Leonards
O. L. Lund
George W. McAlpin
Eugene B. McDonald
James H. McLerran
Thurmul F. McMahon
C. E. Minor
James K. Mitchell
Carl L. Monismith
L. T. Norling
Arnold C. Orvedal
W. A. Raney
Robert L. Schiffman
H. Bolton Seed
J. B. Sheeler
Preston C. Smith
Olaf L. Stokstad
Thomas H. Thornburn
W. J. Turnbull
Reynold K. Watkins
Hans F. Winterkorn
K. B. Woods
Walter H. Zimpfer

DIVISION B

Carl L. Monismith, Chairman
University of California, Berkeley

William P. Hofmann, Vice Chairman
New York State Department of Transportation, Albany

COMMITTEE ON STRENGTH AND DEFORMATION CHARACTERISTICS OF PAVEMENT SECTIONS

(As of December 31, 1968)

Fred N. Finn, Chairman
The Asphalt Institute, Berkeley, California

Richard D. Barksdale
Bonner S. Coffman
B. E. Colley
J. A. Deacon
Hsai-Yang Fang
Raymond A. Forsyth
William S. Housel
W. Ronald Hudson
Wolfgang G. Knauss
Robert L. Kondner
H. G. Larew
Fred Moavenzadeh
Carl L. Monismith
Bryan P. Shields
James F. Shook
Eugene L. Skok, Jr.
Jack E. Stephens
Ronald L. Terrel
Aleksandar S. Vesic

COMMITTEE ON FOUNDATIONS OF BRIDGES AND OTHER STRUCTURES

(As of December 31, 1968)

Philip Keene, Chairman
Connecticut Highway Department, Wethersfield

Edwin C. Beethoven
Harry M. Coyle
Melvin T. Davisson
Jacob Feld
Bedrich Fruhauf
Harry D. Gibbons
Walter W. Grimes
Wayne Henneberger
William C. Hill
William P. Hofmann
William S. Housel
Horace E. Hoy
Martin S. Kapp
Richard E. Landau
Clyde N. Laughter
G. A. Leonards
Alex Rutka
Gregory P. Tschebotarioff

COMMITTEE ON MECHANICS OF EARTH MASSES AND LAYERED SYSTEMS

(As of December 31, 1968)

Robert L. Schiffman, Chairman
University of Illinois at Chicago Circle, Chicago

Richard G. Ahlvin
William Baron
Donald M. Burmister
John T. Christian
Jacob Feld
A. A. Fungaroli
Delon Hampton
Milton E. Harr
R. L. Kondner
Raymond J. Krizek
Charles C. Ladd
Ulrich Luscher
Thurmul F. McMahon
Keshavan Nair
A. M. Richardson
Bruce B. Schimming
Werner E. Schmid
Frank H. Scrivner
Eugene L. Skok, Jr.
Robert D. Stoll
Aleksandar S. Vesic
Harvey E. Wahls
William G. Weber, Jr.
Russell A. Westmann

Foreword

The term "reinforced earth" may be misunderstood prior to reading the article by Vidal, but a study of this novel approach will prove highly interesting. The possibilities in construction application, as already in use in Europe, will immediately appeal to the sense of the practical. Providing the cost savings as shown in Europe can be approximately duplicated in this country, there are many locations where this new method could find useful application. This use of relatively non-cohensive natural soils with light reinforcing to construct vertical embankments is appealing.

Three papers dealing with theoretical stresses and deflections in pavement systems help explore the scientific explanations for pavement action and reaction. Schiffman delves into continuum theories for a rational analysis of pavement behavior explaining the stresses and displacements due to tire load transmitting vertical loads and lateral traction depending upon the adhesion between the tire and pavement. Similarly, Chou and Larew present a study of the response of the pavement system to moving loads. Comparisons are made between the results of this study and field measurements. Gerrard presents solutions for displacement, strain, and stress components produced by circular surface loadings. All three papers serve to extend the knowledge of the mechanics of layers and performance under load. This knowledge will help to define design concepts to provide for improved and lengthened performance of pavements in the field.

James, Krizek, and Baker developed an empirical rule to describe the nonhomogeneous distribution of undrained shear strength with depth for a purely cohesive soil. Designers of footings for retaining walls, bridges, etc., will appreciate the charts and equations that are presented for a variety of strength distributions. One of the conclusions is that the bearing capacity in this study was found to be strongly dependent on the width of the applied load and to a lesser extent on the effect of overconsolidation in the upper zone.

The steady-state seepage flow under and through a leaky sheetpile (and most of them are to some degree) has been studied by Krizek and Karadi by means of an electric analog. Charts are presented to evaluate quantitatively the extent of the decrease in effectiveness in relation to the percentage of holes in the leaky sheetpile.

Contents

The Principle of Reinforced Earth

HENRI VIDAL, Bureau d'Etudes de la Terre Armée, Paris, France

•REINFORCED earth is a material formed by combining earth and reinforcement. The term "earth" covers all types of ground found in nature, or produced by physical or chemical means, including both granular soils and earth which exhibits some slight cohesion.

It can include all particle sizes (silt, sand, gravel, stones, and all sizes of rocks); it can be formed of prefabricated elements (concrete, for example). The word "reinforcement" is used to define all linear components which can withstand major tensile stresses. Thus, earth is a mass of constituents with compact shapes, close to a sphere or cube; as a result, we will call them "grains" or "particles". Reinforcing members are elongated elements, with one dimension clearly greater than the others.

Earth alone, or at least granular earth, according to the definition used in soil mechanics, is made up of non-cohesive particles, but when horizontal beds of flexible, rectilinear reinforcement are introduced into this earth, the whole mass exhibits some cohesion. It is a body of reinforced earth.

This cohesion of reinforced earth arises from friction of grains of earth against the reinforcing members. There is a transmission of forces by friction between the grains and the reinforcements, introducing true cohesion to the whole mass.

This assumes that there is grain-reinforcement friction without sliding; therefore, the reinforcing members must be so arranged that this condition is always met. Since reinforcement can be placed along the directions of the three axes of a trihedral, it can easily be understood that a reinforced earth body may present cohesion in all directions. Consequently, it is possible to build structures of reinforced earth in any desired shape.

In such structures, the stresses developed in the reinforcement depend on the sum of the contact actions between the earth particles. As a result, if the reinforcement is properly placed and designed, it is possible to avoid any shear and any sliding, so that the entire mass behaves like a cohesive solid capable of withstanding both internal and external forces.

In short, friction is the basis of the theory of reinforced earth. Once the proper contact between earth and reinforcement is established, the problem becomes one of calculating the stresses in the reinforcement and in the earth.

FRICTION BETWEEN EARTH AND REINFORCEMENT

To be effective, the reinforcing members must be connected to the earth. Since the reinforcing action results only from friction, it must be determined whether this friction exists without sliding.

Let us consider two grains of earth in contact with a reinforcing member (Fig. 1). If the contact force makes an angle α with the plane perpendicular to the reinforcement (f being the friction coefficient between grains and reinforcement) there must be the relationship $\text{tg}\ \alpha < f$. However, if the tension in a reinforcing member remained constant, it would transmit none of its stress to the earth and have no effect on α or the second grain. It would form no connection between two neighboring grains, such as in the case of tie rods.

Paper sponsored by Department of Soils, Geology and Foundations.

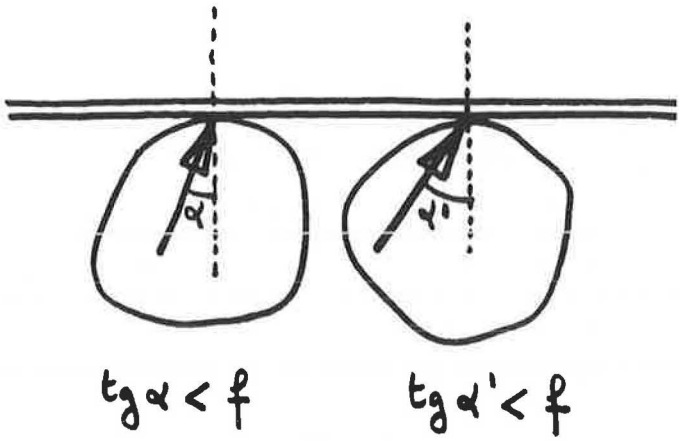

Figure 1.

On the other hand, if the tension in a reinforcing member has a value of F_1 immediately in front of a grain (Fig. 2), and F_2 immediately after the neighboring grain, everything behaves as if the reinforcement were creating a connection between the two grains with a tension $F_1 - F_2$. For this connection actually to take place, this tension $F_1 - F_2$ must result from friction without sliding between the earth and the reinforcement. Let us call dl the distance between the two points where the tension has the respective values F_2 and F_1 (Fig. 3).

Over the length dl of the reinforcement, the stress varies by

$$dF = F_2 - F_1$$

If the stress in the earth perpendicular to the plane of the reinforcement (Fig. 4) has the value N (the force normal to the reinforcement over this length dl), and on two faces a value of 2 Ndl; it is then necessary to ascertain that friction is taking place without sliding, or

$$\frac{dF}{2\,Ndl} < f$$

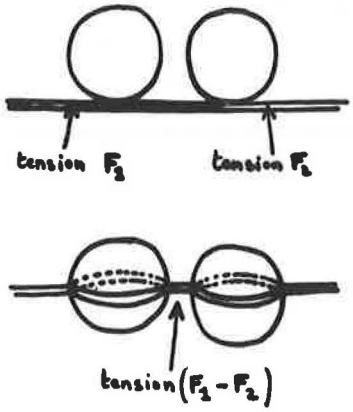

Figure 2.

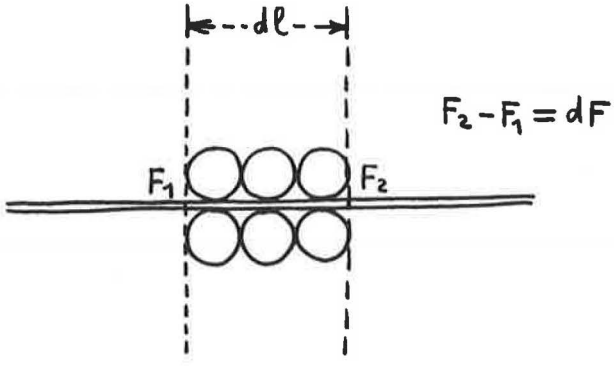

Figure 3.

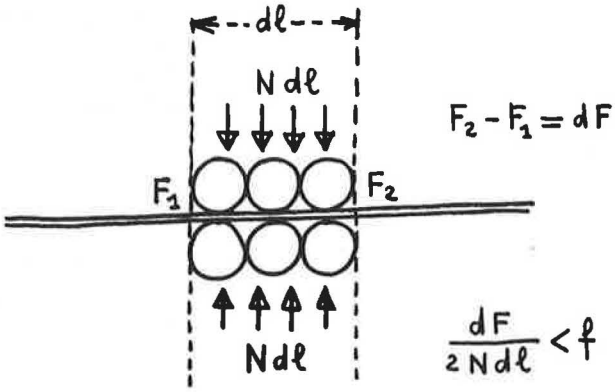

Figure 4.

Since f is the coefficient of friction between earth and reinforcements, the coefficient 2 results from the friction on both faces of the flat reinforcement. As a result, if the relationship

$$\frac{dF}{2\,Ndl} = \frac{f}{s}$$

is verified, it can be assumed that granular friction on either side of the reinforcement is taking place without sliding, and with a factor of safety, s.

This relationship is somewhat similar to that of the bonding of the reinforcement in a reinforced concrete beam, only the bond stress is replaced by a pressure multiplied by twice a coefficient of friction. This formula assumes that the reinforcing members are flat and that a layer of reinforcement forms a complete plane. In reality, the reinforcements are in flat bands of limited width spaced at finite distances from each other (Fig. 5).

If K is the proportion of reinforcement per unit length, the formula becomes

$$\frac{dF}{dl} < 2\,KNf$$

The slope of the curve giving the stress in the reinforcing members as a function of their length must not exceed a certain value. In the case of the beam in reinforced earth with a shear force T, $dF/dl = T$, and it is enough to assure that

$$T < 2\,KNf$$

In the case of round reinforcements (Fig. 6), a similar formula will apply:

$$\frac{dF}{dl} < K\,\pi\,\phi\,Nf$$

where

ϕ = diameter of rod,
K = number of rods per unit, and
N = average pressure around the rod.

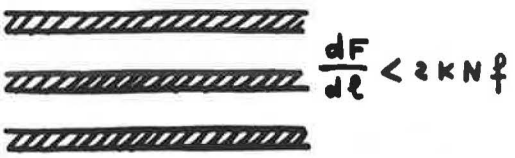

Figure 5.

These two formulas are pessimistic because they do not take into account the arching effect between adjoining reinforcing bars.

In the preceding arguments, only the connection between a reinforcing member

Figure 6.

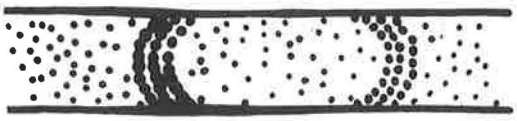

Figure 7.

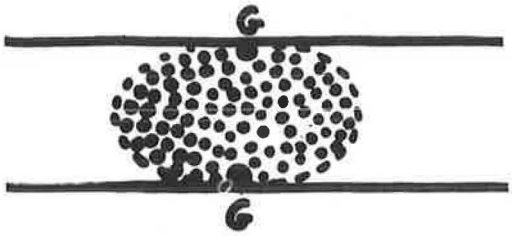

Figure 8.

and the grains of earth with which it has direct contact has been considered, but reinforcing layers generally lie at some distance from each other. Therefore, we must examine the manner in which the stresses in the reinforcement are transmitted from the grains in direct contact to those not in contact.

Although the manner of transmission is not known with certainty, it is assumed that this connection must be in some form of a strut or arch (Fig. 7). However the lack of such knowledge in the case of reinforced concrete has not hindered its development in the last 50 years.

In reinforced earth it is assumed that a grain G directly in contact with the reinforcement has an appreciable effect only on the grains between two layers of reinforcement over a certain radius related to the spacing of the reinforcing members (Fig. 8). Therefore, in making calculations, the earth particles can be considered as sacks of earth with a thickness equal to the distance between two reinforcement layers.

It is of little importance that we do not know exactly what happens within the sacks. If a structure actually consisted of sacks of earth, all the calculations would still be fully justified; opening the sacks by tearing the sides perpendicular to the reinforcement (Fig. 9) need not change the distribution of the stresses except in the immediate neighborhood of the tear. This should make no difference to the stresses on a grain A situated in the middle of the sack (Fig. 10).

Thus, it can be seen that the first condition for the existence of reinforced earth—friction between earth and reinforcement—can be met, and it can be checked by verifying a relatively simple formula. The calculation depends on the coefficient of friction between the earth and the reinforcement, on the stresses in the earth, on the geometric properties of the reinforcement, and on the rate of change of tension along each reinforcement.

Contrary to what might be thought, this condition of friction between earth and reinforcement has been achieved in all the numerous works which have been designed.

CALCULATION OF STRESSES IN EARTH AND REINFORCEMENT

It is now necessary to calculate the tension at each point in each reinforcement, together with the stresses in the earth, in order to verify that the mass always remains in equilibrium. Difficulty in calculating reinforced earth results from dealing with

Figure 9.

Figure 10.

a heterogeneous material that is generally non-isotropic and which, to all appearances, includes large plastic zones.

Although these special characteristics do not interfere with the validity of Mohr's circle, which makes it possible to represent the stresses in the earth around a point, it seems difficult at first to connect the stresses and strains in some simple manner—such as the theory of elasticity or of strength of materials. Nevertheless, reinforced earth can be calculated and may be considered as a material having a certain elasticity.

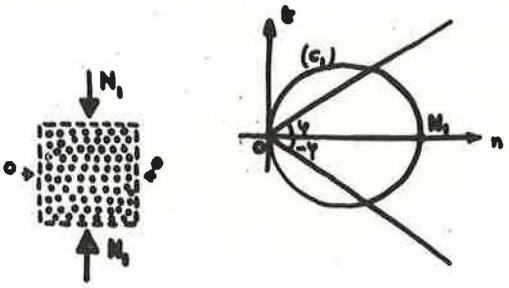

Figure 11.

As a first step, the fundamental cases of simple compression and tension will be studied. Then the elasticity properties of reinforced earth will be discussed, together with two methods of calculating the stresses in the most general case.

Pure Compression

Material formed by a mass of particles without reinforcement has properties that are identical in all directions, since the particles are in a random arrangement. Therefore, the theory of the intrinsic curve (formed of two straight lines inclined at $+\varphi$ and $-\varphi$) is applicable.

A cube of earth (Fig. 11) subjected to a compressive stress N_1 on its two faces cannot remain in equilibrium, because the corresponding Mohr's circle (C_1) cuts the intrinsic curve. The cube can only be stable when compressive forces, N_2, which are at least equal to $i\,N_1$, act on its other faces (Fig. 12). As a function of the angle of internal friction, the coefficient of active lateral earth pressure, i, has a value of

$$i = \tan^2\left(\frac{\pi}{4} - \frac{\varphi}{2}\right)$$

Mohr's circle (C_2) then becomes tangential to the intrinsic curve. In the absence of reinforcement, these stresses N_2 can only be produced by external forces. It is no longer a case of simple compression, but of restrained compression.

Let us now examine how the reinforcement produces stability in a cube of reinforced earth subjected to simple compression.

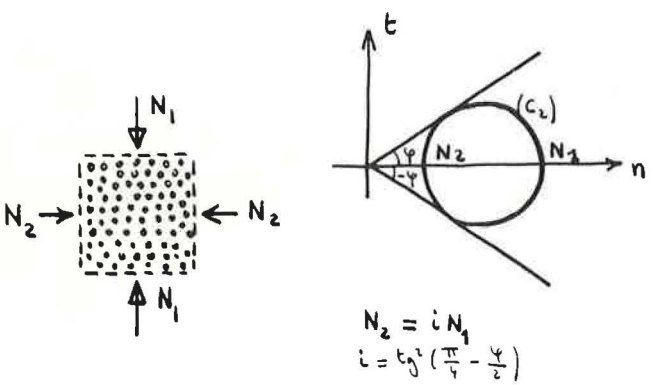

Figure 12.

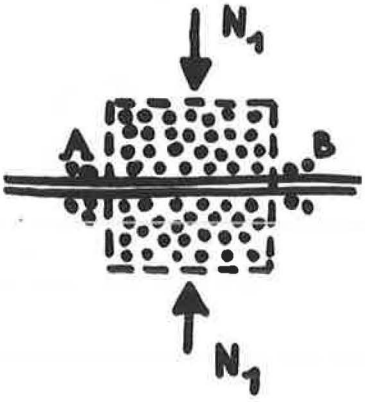

Figure 13.

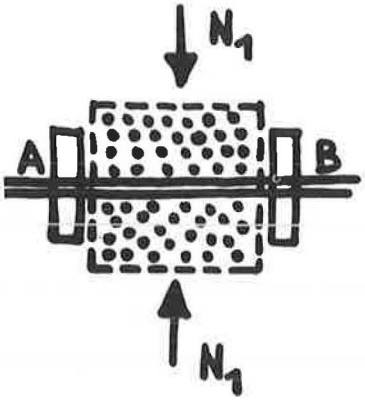

Figure 14.

When considering an elementary cube of reinforced earth (Fig. 13), it is assumed that the reinforcement is arranged perpendicular to the direction of the compressive force N_1 in two directions at right angles. For this reinforcement to fulfill its function, it is assumed that there is no sliding between the reinforcement and the particles. Thus, the neighboring particles A and B are rigidly connected by the reinforcement.

If A and B are contained in the two portions of earth nearest to two faces of the cube (Fig. 14), but outside this cube, everything acts as if the two plates formed of the external particles, which can produce stress on these two cube faces, were connected by the reinforcement.

When the simple compressive stress N_1 is acting and when there is no compressive stress on the particles in the direction AB, sliding of the particles with respect to each other is automatically produced, since Mohr's circle passes outside the intrinsic curve (Fig. 15). The particles in the cube are in a plastic state.

But the elementary cube tends to compress in the direction of compression, and since the particle mass occupies a volume which is roughly constant, it tends to expand in the direction of the reinforcing members (Fig. 16). These expansions of the earth in the direction of the reinforcement are accompanied by extensions of the reinforcement. As a result, compressive forces, caused by the interconnection of the particle plates on either side, act on the faces of the cube.

The sliding of the particles within the cube is interrupted when the compressive forces become equal to $i\,N_1$ in such a way that Mohr's circle becomes tangential to the

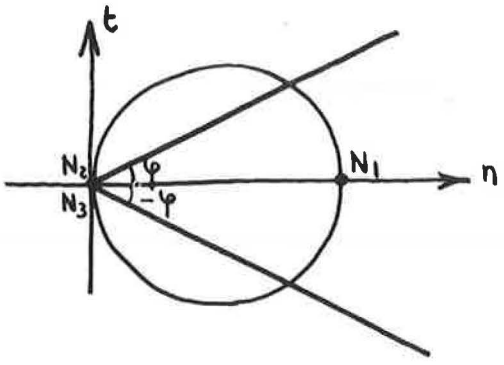

Figure 15.

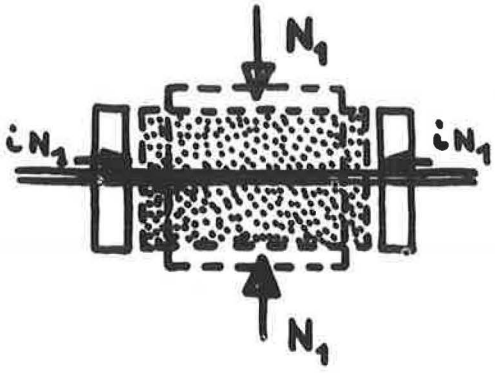

Figure 16.

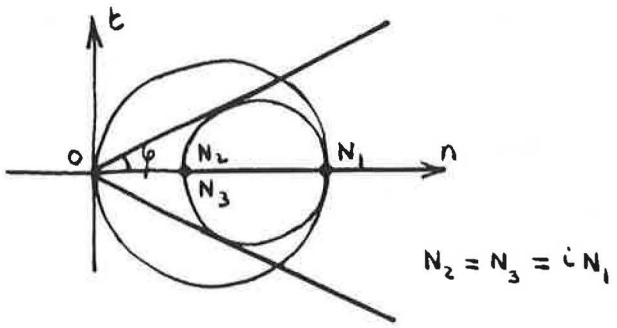

Figure 17.

intrinsic curve (Fig. 17). The complete reaction is that of an elastic body in compression, with a modulus of elasticity

$$E_t = \frac{ES}{2i}$$

where

E = modulus of elasticity of the reinforcements,
S = cross-sectional area of the reinforcements per unit area of earth, and
i = coefficient of active lateral earth pressure.

Pure Tension

In the case of pure tension, resistance to tension is provided only by the reinforcements. Assuming that there is no sliding of the particles with respect to the reinforcements, reinforced earth is elastic in simple tension, as if the reinforcement were there by itself, the modulus of elasticity being ES (E = modulus of elasticity of the reinforcement; S = cross-sectional area of reinforcement in tension per unit area of earth).

Elasticity of Reinforced Earth

As long as there is no sliding between the particles and the reinforcement, reinforced earth has an elastic behavior which is as effective in tension as in compression, but its elasticity is not the same in the two cases. Even if the density of reinforcement were uniform at all points and the same in all directions, the modulus of elasticity in tension would generally differ from the modulus of elasticity in compression, but not to a great degree. In practical applications this modulus of elasticity is generally small. Thus, although it may seem paradoxical, earth will often be as elastic as timber or reinforced concrete.

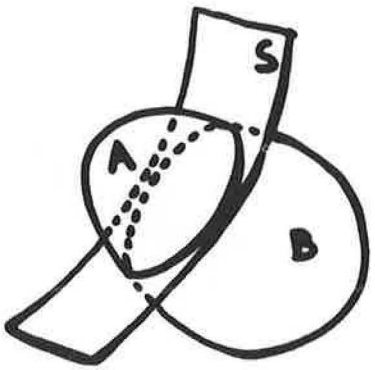

Figure 18.

But if earth shows elastic properties, it follows (in a very approximate way) the mathematical theory of elasticity, since the constant ratio between stresses and strains can vary with the direction of the stress and with the point under consideration. In tension, it varies with the area of longitudinal reinforcements; in compression, it varies with the section of transverse reinforcement. The exact mathematical theory of elasticity in the case of a non-isotropic material includes

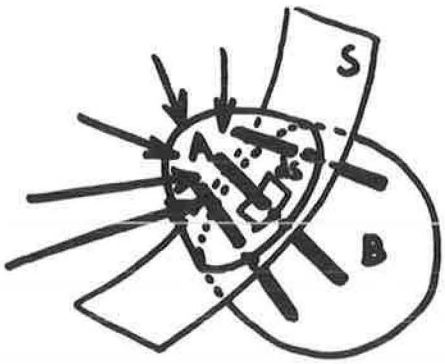

Figure 19.

too many parameters to permit its practical use without complicated calculations.

In fact, reinforced concrete also does not have the same elasticity in tension as in compression; moreover, in compression the elasticity of concrete varies with the value of the stress. Thus, there is never any proportionality between the forces and deformation at any point for a given direction, although this proportionality does exist for reinforced earth.

It should be remembered that when demonstrating the elasticity of reinforced earth in compression and in tension, it has been assumed that the particles were sufficiently compacted to eliminate cavities, so that during deformation the volume of a unit cube remained more or less constant. In actual practice, such may not always be the case, and the period of apparent elasticity of the reinforced earth may be preceded by a period during which collapse of the cavities and compacting of the grains produces an initial, non-elastic, permanent deformation, which would appear, for example in the case of a beam, as a permanent deflection.

The Design of Structures of Any Shape

For structures of any shape, two methods of design have been prepared.

First Method—In the first method, which is more practical, the volume of reinforced earth is cut by a surface S (Fig. 18) which divides it into two parts A and B. To prevent volume A from slipping with respect to volume B along surface S, under the action of forces acting on A and B, it is generally necessary to provide reinforcement connecting A and B. This reinforcement must be so arranged that there is no sliding of any element of surface dS anywhere on area S (Fig. 19).

Thus, it is assumed that over an element of surface dS, the result of the forces of A on B is R_1, making an angle greater than φ (Fig. 20) with the normal to dS. It is possible to arrange reinforcement connecting volume A to volume B with a tensile force F such that the resultant R_2 of R_1 and F makes an angle less than φ (Fig. 21) with the normal to dS.

Inasmuch as this arrangement can be provided for all the surface elements dS of the area S, reinforcement can prevent the sliding of A on B, and the size and spacing

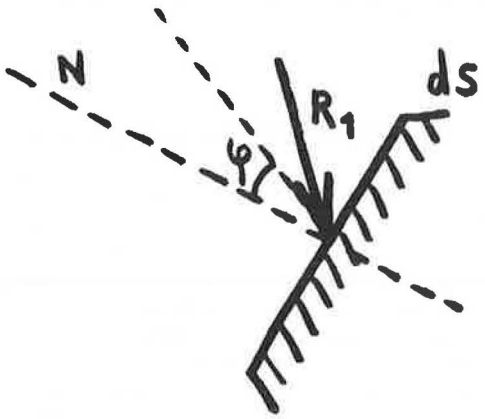

Figure 20.

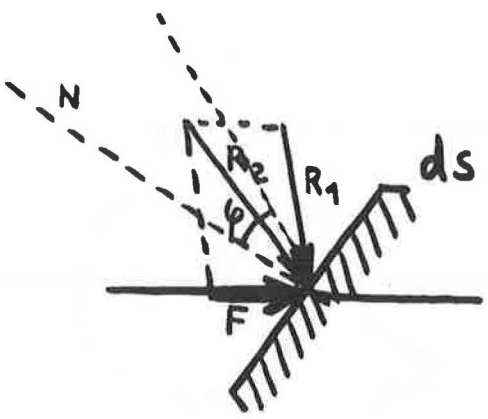

Figure 21.

of reinforcement necessary at each point can easily be calculated.

If this equilibrium condition can be achieved, for any area S cutting the volume of reinforced earth, then the entire mass will be in equilibrium.

In practice, the surface S is replaced by planes, and earth stresses in these planes are usually known with sufficient accuracy by assuming a linear distribution of forces of contact along these planes.

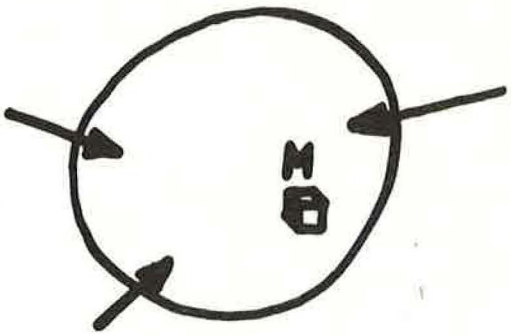

Figure 22.

Second Method—The second method calculates the stresses by the theory of elasticity (Fig. 22). A body of reinforced earth is elastic according to Hooke's law, that is to say that at a point M the deformations are linear functions of the stresses. For a body of any shape, it would theoretically be possible to determine the stresses at any point, as functions of the external forces—as if the body were following this law of elasticity. This law, moreover, takes into account the arrangement and size of reinforcement within the volume under consideration. In practice the calculation would generally be almost insoluble.

On the other hand, elastic calculations in which the materials are assumed to be isotropic and homogeneous are conventional calculations in a certain number of simple cases. For cases of complicated volume, the stresses and strains may be evaluated by photoelasticity.

Finally, in the case of an elongated body which can be compared to a beam, the stresses may be calculated still more easily by the theory of strength of materials.

It is thus tempting to try to apply the conventional theory of elasticity to a body of reinforced earth, if one could be sure that this comparison did not lead to major errors.

But it is even more tempting to do so, when one sees this theory of elasticity currently applied to concrete, which is not elastic since its deformations do not vary in a linear way with respect to the stresses; it is sometimes applied to reinforced concrete; and it is applied to many other non-isotropic materials.

If the stresses at any point are known in the case of an elastic body, according to the forces acting on the body, it becomes a question of seeing how these imaginary stresses make it possible to determine the stresses in the earth and in the reinforcement. These imaginary stresses at any point M may be represented by the corresponding Mohr's circle, C′ (Fig. 23). Since there is generally no reason for this circle to lie inside the intrinsic curve for the earth, equilibrium will not generally occur with granular earth.

Inclusion of reinforcement modifies the stresses in the earth in such a way that the new Mohr's circle at this point, corresponding to the earth alone, lies inside the intrinsic curve.

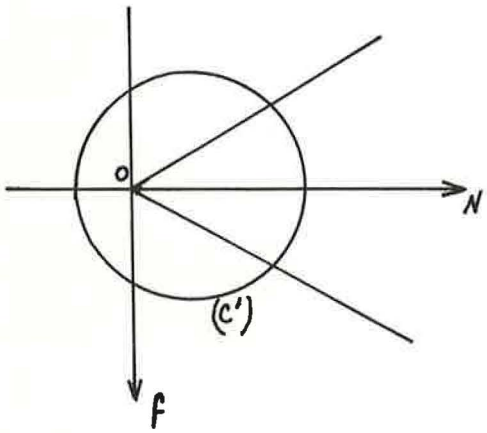

Figure 23.

Figure 24.

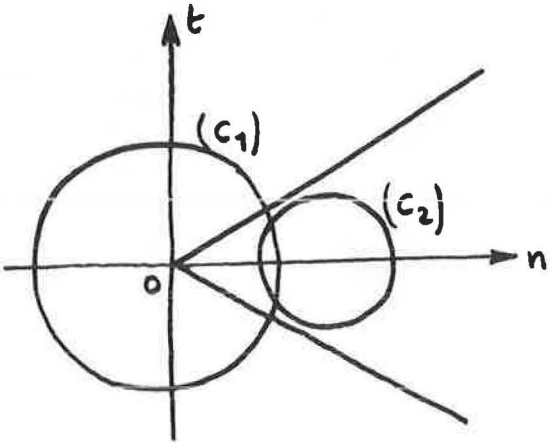

Figure 25.

In practice, during the course of general elastic deformation, the particles cannot remain in equilibrium without reinforcement, and slide in such a way that the reinforcement is placed in tension (Fig. 24).

If it is assumed that the connection at A and B between the particles and the reinforcement is done without sliding, and we have concluded that everything acts as if the two faces A and B of the elementary cube of earth formed two plates rigidly connected to the reinforcement.

The reinforcement is placed in tension between A and B with a tensile force F equal to the compressive force exercised by the plates on the grains. Thus, the effect of the presence of the reinforcement is to introduce an additional compressive force in the grains, parallel to the reinforcement and equal to the tensile force in the latter; the corresponding compressive stress has a value of n_a such that F equals S n_a, where S is the area of action of the reinforcement on the particles perpendicular to the direction of the reinforcement.

Taking into account this additional compression in the earth, a new Mohr's circle can be drawn (C_2) which represents the stresses in the earth alone around the point considered (Fig. 25). For the earth to be in equilibrium, this new Mohr's circle must lie inside the intrinsic curve for the earth.

The graphical construction which makes it possible to find the value F of the stress in the reinforcement is simple, and this method can be used to calculate all the stresses in the reinforced earth body.

CONCLUSIONS ON THE THEORY OF REINFORCED EARTH

The fundamental calculation for the friction between earth and reinforcement, which is the basis of the cohesion of reinforced earth, is extremely simple. When the stresses in the earth and the reinforcement are known, only a simple formula is needed for computation.

Insofar as the calculations for the earth and the reinforcements, it can be said that they are fairly close to the calculations which are made for conventional structures and materials.

The principal cases of pure compression and pure tension are calculated with the same degree of accuracy as for conventional structures. On the other hand, for work of no specified shape the calculations are fairly difficult—as is the case with other materials.

It is because structures of this nature may be encountered fairly frequently in reinforced earth that the two very different methods have been prepared for their design. And when these two methods have been applied to the design of the same work, the results have been very close in agreement.

But there is one point at which reinforced earth leaves all conventional materials far behind. This is the possibility of checking the most difficult calculations by means of scale models. These scale models are very simple to construct, and they will always offer a very effective method of checking the theoretical calculations. Therefore, they should advance the accuracy of this theory.

CONSTRUCTION OF REINFORCED EARTH STRUCTURES

In actual construction, the reinforced earth structures are composed of earth and reinforcing elements in the form of strips disposed in horizontal layers. In these

layers, the strips are set at certain intervals. On the facing of the structure, a certain type of boundary, or skin, is required to retain the earth particles that are not in contact with reinforcing strips.

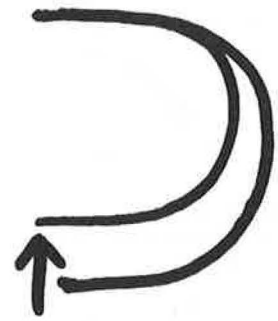

Figure 26.

The Skin

The skin must have certain qualities. First, it should have sufficient local resistance to retain the particles of earth contained between two adjacent reinforcing members close to the surface. But it must also have sufficient flexibility to follow all deformations of the mass, by forming an integral part of the mass. If the skin were rigid, it would find itself in contact with members external to the reinforced earth mass—the supporting ground for example. It would also transmit large additional external forces (about which little would be known and which would make it necessary to increase its rigidity even more). This would completely deprive the reinforced earth of its homogeneous quality.

Thus, walls made with sheet piling with tie rods and anchoring blocks are not reinforced earth structures, because their tie rods (wherein the tension is constant) have no similarity with reinforcement in which the tension varies and which links together particles in the earth mass.

The boundary skin must have the particular property of adequate local resistance, combined with overall flexibility. It must act as a protection by offering resistance to shock and abrasion; it must be in a material or of a color which is acceptable. It must be of a sufficient degree of tightness or must provide drainage. It must be designed in such a way that its placing, together with that of the earth and the reinforcement, is very simple. Finally it must have a high resistance to corrosion.

The skin may be plane, and may deflect through the simple elasticity of the material, just like rubber sheets. It can also be formed of rigid elements overlapping one another, as in the shells of numerous insects or crustacea (and there are several types of skin derived from this idea). But it may also be flexible by making use of curved areas (Fig. 26) with overall flexibility due to large curved surfaces.

The semi-elliptical cylindrical elements or skins arise from this principle. Starting with this basic element, it is always possible to construct a body of any required size in reinforced earth, because the surface of the body can always be broken down into a pattern of elementary rectangles (Fig. 27). This basic element, which can have widely differing dimensions, is economical since it works in tension under most filled conditions. It is stable, and its stability is guaranteed regardless of the forces in the earth, its characteristics, or its settlement.

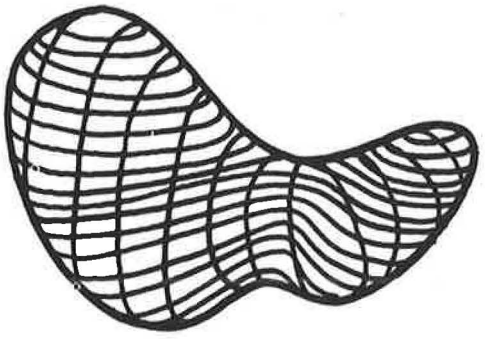

Figure 27.

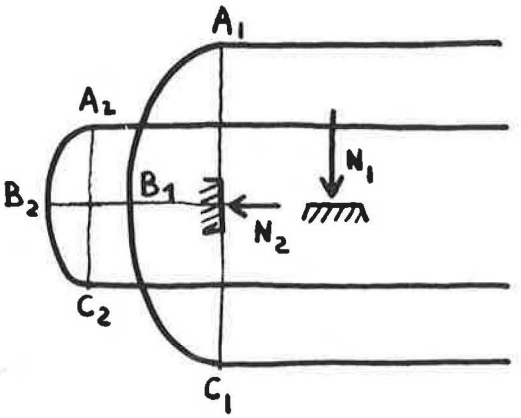

Figure 28.

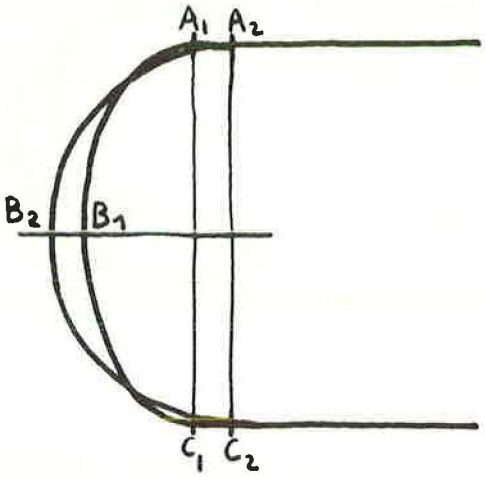

Figure 29.

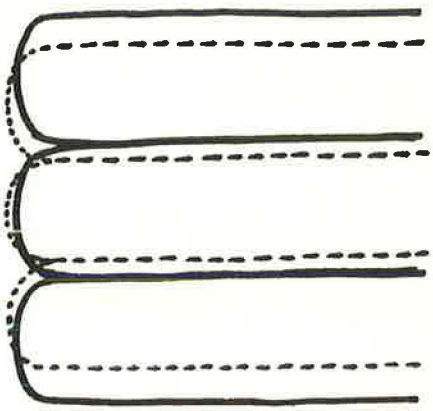

Figure 30.

The result can be shown on a scale model (Fig. 28). It can also be demonstrated mathematically by making the assumption that the stresses in the earth contained inside a skin element comply with a state of equilibrium similar to that of Rankine; that is to say, that the principal directions N_1 and N_2 are at all points parallel and perpendicular to the general line of the surface of the skin, and that the ratio of these principal stresses $N_1/N_2 = i$ is constant.

Under these conditions it has been verified, by the membrane theory, that the stable shape for a skin member is a semi-ellipse, with a ratio between the axes of $\sqrt{i}$.

When the value of i changes (Fig. 29), or does not comply with $\varphi = 30$ deg, chosen for the initial ellipse, the ellipse changes shape slightly until the ratio between the axes returns to $\sqrt{i}$, corresponding to the actual angle of friction of the earth. In practice, these two phenomena occur at the same time, and there is an adjustment with a change in the value of i (Fig. 30). The local radius of curvature of the skin then varies enormously.

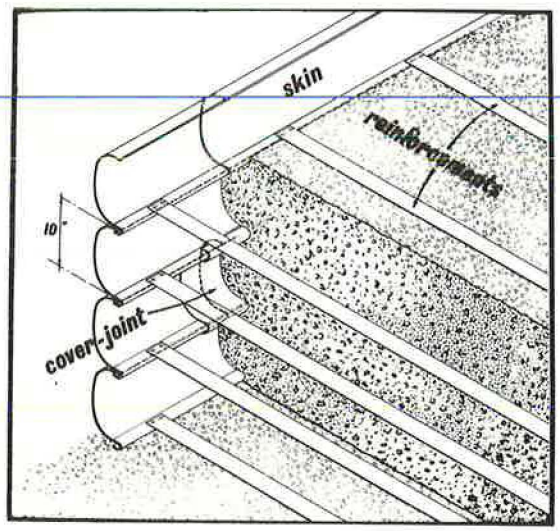

Figure 31.

It has been verified that with this special form it is possible for this deformation to take place and still give a factor of safety which is always greater than 2. This holds true no matter what the material chosen and for high values of skin tension. It is concluded that, from a purely mechanical point of view, the skin needs only a very small thickness to resist the forces acting on it. Other factors, such as corrosion, lead to increased skin thicknesses.

Corrosion is a factor to be taken into account. Galvanized steel or aluminum magnesium alloy have already been used in structures. Plastics have been tested. In the future, new types of metals, such as weathering steels, will certainly be used.

Outside the initial protection given by a coating such as galvanization, or various types of chemical coatings, one way to fight corrosion is to in-

troduce in the skin and reinforcements the necessary extra thicknesses of metal.

As previously shown, only small metal thicknesses are necessary from a purely mechanical point of view. Generally speaking, the metal in reinforced earth structures is under low stress, whereas sheet or tube piling is under high stress and corrosion can rapidly become dangerous.

Thus, the metallic elements of reinforced earth can be calculated to last the design life of the structure.

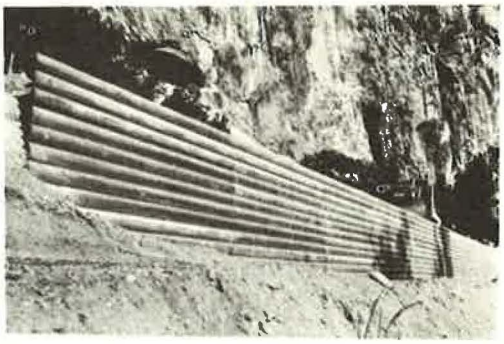

Figure 32.

Reinforcing Elements

Reinforcing elements can be made out of any material possessing the necessary tensile strength and in any shape giving the necessary friction surface in the required direction. Thus, strips, wire mesh, steel cables, aluminum alloy or plastic fabric have been and could be used. Most construction for walls has used elongated reinforcing strips made of galvanized steel or aluminum magnesium alloy. The strips are disposed in horizontal layers and tied to the skin elements (Fig. 31). They are set at calculated distances, depending on the forces acting on the structure.

The Earth

Between two horizontal layers of reinforcing strips, earth is dumped and, depending on the purpose of the structure, can be compacted or not.

"Earth" as used in this paper covers a great number of natural soils, composed mostly of granular material, with an amount of clay not exceeding a certain limit. This limit varies with the type of reinforcement used, the general condition being that sufficient friction exists between earth and reinforcement to generate the necessary tensile stresses in the reinforcement. With the conventional type of reinforcement generally used, this condition is met with earth having an international friction angle around 25 degrees.

When building reinforced earth structures, conventional testing methods for embankment materials are used.

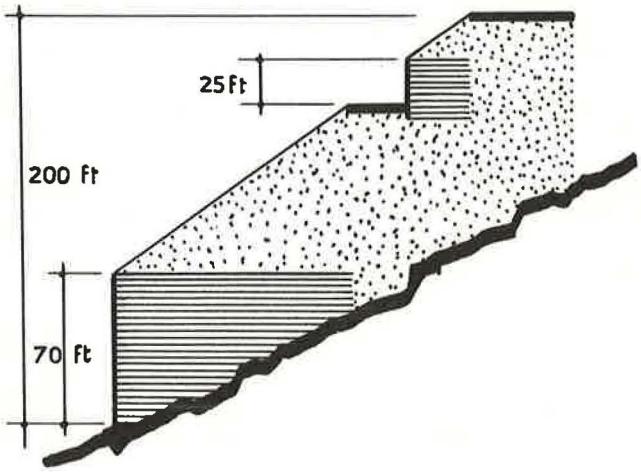

Figure 33.

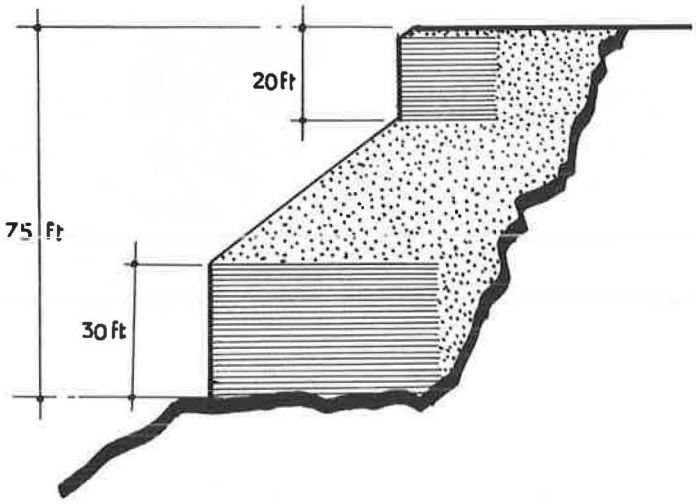

Figure 34.

Types of Reinforced Earth Structures

Most types of heavy foundation works can be built with reinforced earth as well as with concrete, the respective weights of these two materials being quite close. Thus, the volume of a reinforced earth structure can be similar to that of a comparable concrete one.

Earth-Retaining Walls—Figure 32 shows a typical wall, such as those on French-Italian or Normandy highways, constructed as an embankment to retain the adjoining land—thus reducing the necessary right of way.

Slope-Retaining Structures—Reinforced earth structures can be built on flat ground or on slopes (Fig. 33). The Peyronnet structure on the French-Italian highway was built to retain a large slope, 200 ft in height; an intermediate reinforced earth wall was built in the top section of the slope to provide a service road.

Platform-Supporting Structures—Figure 34 shows a typical example. The Vigna works, on the French-Italian Highway, consists of two reinforced earth walls, the top wall directly supporting the highway platform. The surcharge caused by the highway is taken into account in calculating the distribution and size of the reinforcements inside the structure. It is always possible to design a reinforced earth structure to support whatever external forces are exerted upon it.

Beams and Foundation Mats—The reinforced earth principle has been used in two works of this kind. One is a foundation mat to support a canal that had to pass over a section of ground containing gypsum beds where cavities could be expected to form due to flowing. The other is a roof over a uranium mine in Gabon. Both structures were made with wire mesh as reinforcement inside a mass of granular soil.

Underwater Structures—Underwater structures can be built with the same elements, using an aluminum magnesium alloy to prevent corrosion when working in seawater. Prefabricating techniques have been used to speed up the work, and entire wall panels, including skin elements and reinforcing strips, have been assembled on land and set in place under water as a unit.

Sand is then poured and the reinforcing strips released layer by layer (Figs. 35 and 36). Piers for harbors have been built in France, using prefabricating techniques.

Many other structures with varying shapes and sizes could be built. Walls to support highways or railways in urban areas, dams, cofferdams, and tunnels in embankments have been projected or tested, and calculations have been developed.

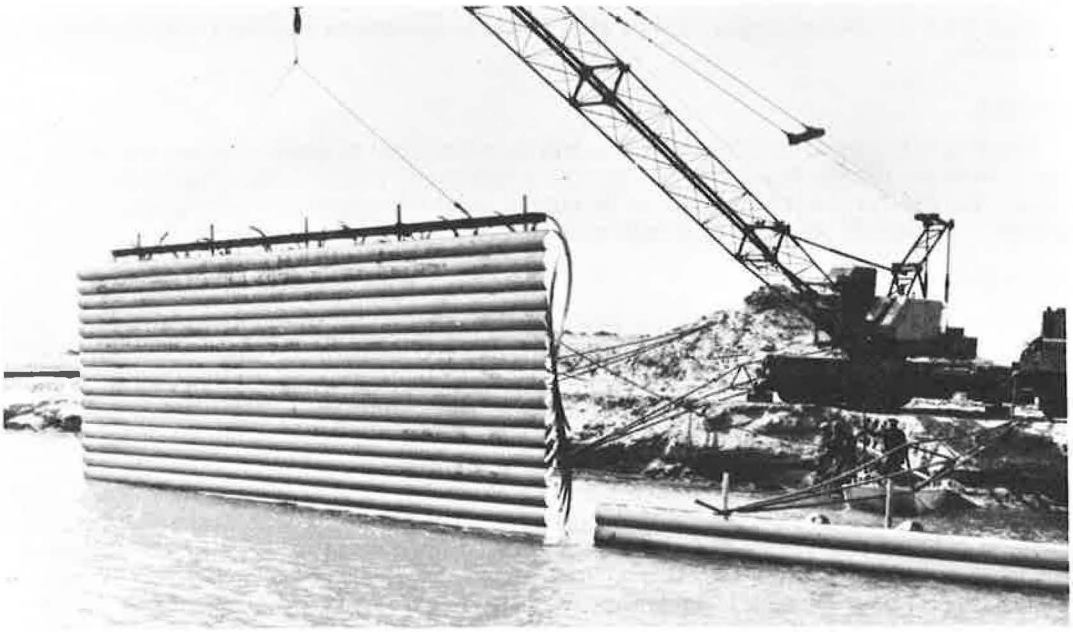

Figure 35.

REINFORCED EARTH PROPERTIES AND ENGINEERING PROBLEMS

The development of reinforced earth in civil engineering is recent; the first structures were built in 1964. Its use as a construction principle arises from several characteristics and indicates the place it is apt to fill in the future.

Heavy Weight

Reinforced earth is a heavy material like concrete. Heavy, solid structures able to resist high stresses or impact loads are often necessary and sometimes desirable for purely architectural reasons. Earth itself is being used in embankments, dams, highway supports, etc., but it requires handling large volumes and results in structures that occupy considerable surface lands that become costly in populated areas.

Reinforced earth has basically the same qualities, but with their vertical

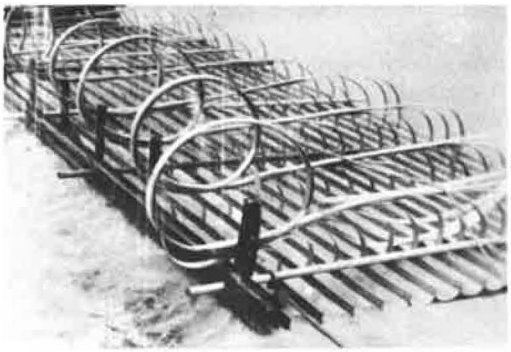

Figure 36.

Figure 37.

facings such structures reduce the amount of earth movement and the right-of-way necessary.

Strength

Unlike earth alone, reinforced earth can be calculated to resist almost any pressure, because the particles constituting the mass usually have a high crushing resistance, and the reinforcing strips can be placed inside the mass to resist external conditions. Figure 37 shows a very high wall built with a large safety factor.

Flexibility

The mass constituting reinforced earth being essentially granular in nature, deformations of the supporting foundation do not produce fissures or breaks, as would be the case with concrete. In fact, an infinite number of fissures or cracks exists in the mass, and movements of the ground cause these fissures to move. In such a case, the particles slide along the reinforcing elements to achieve another state of equilibrium—resulting in another stress distribution in these elements.

As long as the reinforcing elements are calculated to withstand these new loads, the whole structure remains stable. This phenomenon of plasticity with large deformation prior to rupture is an essential quality of every building material. Properly designed reinforced earth can possess this quality to such a high degree that resistance to earthquakes should be important. Naturally, stability to external forces induced by earthquakes should be considered, but reinforced earth should be more econimically favorable than conventional materials because of the necessity for a large horizontal base and inside dimensioning.

Simplicity

Building reinforced earth structures is simple and fast. There is no time factor for settlement and compacting is necessary only when it is desired to limit vertical settlement. Skin elements come in standard length, are easy to handle, and no heavy equipment is necessary. No special skills are required either.

Economy

Because of its relative simplicity, the economy achieved in comparison with concrete is great. The forces inside the mass of a structure are resisted by reinforcing elements placed according to calculations, and only in the direction required by the action of external forces. Concrete construction requires cement in all directions, making for an expensive and wasteful use of cohesive forces.

In French highway experience, reinforced earth structures cost approximately half what concrete structures would have cost for comparable uses. They were also less costly than all other types of retaining walls (crib or bin walls) that could have been used.

There is no height limit to structures made with the reinforced earth principle, and, indeed, its economic advantage increases with the height.

With these interesting characteristics, the reinforced earth principle can be expected to be used extensively in construction all over the world, filling a place between the large, heavy earth or concrete gravity works, and the ultra-elaborate reinforced or prestressed concrete structures.

Finally, it should be pointed out that the reinforced earth principle, and its applications, are patented in the United States and most other countries.

The Influence of Adhesion on the Stresses and Displacements in an Elastic Half-Space

ROBERT L. SCHIFFMAN, University of Illinois at Chicago Circle

•A RATIONAL analysis of pavement structures, foundations and land locomotion problems is based on the application of continuum theories of behavior of pavements and/or soil systems. The objective of a rational analysis is the development of numerical data that will accurately predict the performance of a particular engineering structure. In the analysis of pavements this objective would be accomplished if the rational analysis accurately predicted the stress and displacements in a pavement system subjected to a known pattern of vehicle loading.

One of the features required in a rational analysis of pavement structures is the description of surface conditions imposed by vehicle traffic. In particular, attention is directed to the lateral restraints imposed on the surface by a tire.

The movement of an automobile, truck or any self-propelled vehicle depends on the traction of the wheel as applied to the pavement surface. A perfectly smooth surface would provide no traction and there would be no movement. Thus, realistically the loaded area of a tire imprint transmits vertical loads due to the weight of the vehicle and tractions which are due to the lateral restraints between the tire and the pavement.

The nature of lateral restraint between the applied tire load and the pavement surface is demonstrated in Figure 1. A static circular loading applied to a frictionless surface (Fig. 1a) will produce a surface displacement vector (u_i). This vector has two components, the vertical displacement (u_z) and the radial displacement (u_r). In actuality, the pavement surface is not frictionless. There is some lateral restraint between the tire and the surface. The application of a vertical force and subsequent lateral motion (u_r) will induce a frictional force between the tire and the pavement. This frictional effect (Fig. 1b) alters the magnitude and distribution of the displacement of the pavement surface. The exact shape of the altered displacement pattern depends on the magnitude and distribution of the frictional force. A simplified means of determining the frictional force is to assume Coulomb friction. The frictional force is then directly proportional to the applied load. A more realistic, though more complex, mechanism would be to consider the frictional force as related to the radial displacements. This is in the nature of considering the adhesion between the tire and the pavement surfaces.

The adhesive effect (Fig. 1c) restricts the lateral displacement (u_r) of the pavement surface. The exact nature of adhesion between the tire and the pavement is unknown. It is probably a function of the load as well as the material properties of tire and pavement. A specification of full adhesion ($u_r = 0$) under the load, on the other hand, will produce an extreme effect which can form a bound to all other solutions.

This paper treats the problem of an elastic half-space. The surface of the half-space is subjected to a vertical loading and a lateral restraint. The vertical load is uniformly distributed over a circular area. The lateral restraint conditions are such that the region inside the circular area has full adhesion (the lateral displacement is zero) while the area outside the circle is frictionless (the shear stress is zero).

ADHESION UNDER A FLEXIBLY LOADED AREA

The theory considered is the three-dimensional theory of elasticity for a homogeneous, isotropic material. Small strains are assumed. It is further assumed that the

Paper sponsored by Department of Soils, Geology and Foundations, Division B.

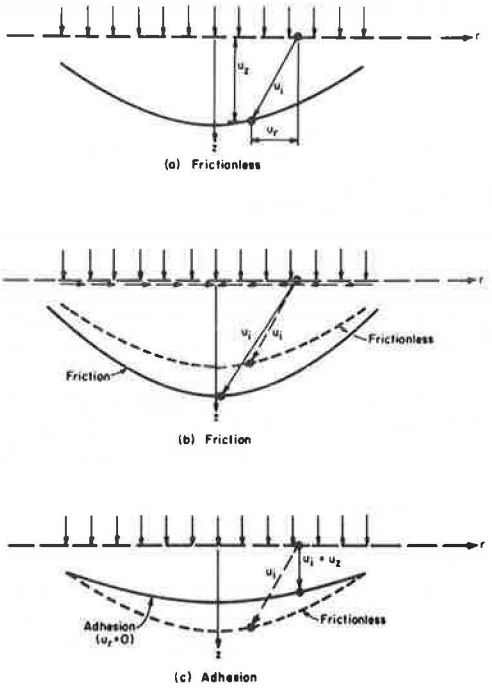

Figure 1. Surface conditions.

elastic medium is a half-space and that the surface conditions induce axially symmetric stresses and displacements. The theory of elasticity sign convention is used. Tensile stresses are positive.

Frictionless Surface

The problem of a frictionless surface was first solved by Boussinesq (1), and later by Love (4). This solution forms the basis for later adhesive surface solutions.

In order to distinguish this solution from others presented here, the stresses and displacements for a frictionless surface will be designated with a superscript (f).

The surface is loaded by a uniform load intensity (p_0) which acts over a circular area of radius (a). The boundary conditions are

$$\sigma^f_{zz} = -p_0, \quad 0 \le r \le a, \quad z = 0 \tag{1a}$$

$$\sigma^f_{zz} = 0, \quad r > a, \quad z = 0 \tag{1b}$$

$$\sigma^f_{rz} = 0, \quad 0 \le r \le \infty, \quad z = 0 \tag{1c}$$

It is convenient to express the stresses and displacements in nondimensional form. The nondimensional variables are

$$R = r/a \tag{2a}$$

and

$$Z = z/a \tag{2b}$$

The stresses and displacements are

$$u^f_R/a = \frac{p_0(1+\nu)}{E}\left[ZI^1_1 - (1-2\nu)I^0_1\right] \tag{3a}$$

$$u^f_Z/a = \frac{p_0(1+\nu)}{E}\left[2(1-\nu)I^0_0 + ZI^1_0\right] \tag{3b}$$

$$\sigma^f_{RR}/p_0 = ZI^2_0 - I^1_0 + \frac{1-2\nu}{R} I^0_1 - \frac{Z}{R} I^1_1 \tag{3c}$$

$$\sigma^f_{\theta\theta}/p_0 = \frac{Z}{R} I^1_1 - 2I^1_0 - \frac{1-2\nu}{R} I^0_1 \tag{3d}$$

$$\sigma^f_{ZZ}/p_0 = -I^1_0 - ZI^2_1 \tag{3e}$$

$$\sigma^f_{RZ}/p_0 = -ZI^2_1 \tag{3f}$$

where

$$I_s^q = \int_0^\infty \lambda^{q-1} J_s(R\lambda)\, J_1(\lambda)\, \exp(-\lambda Z)\, d\lambda \tag{3g}$$

and (E) and (ν) are Young's modulus and Poisson's ratio, respectively.

The integrals (I_s^q) defined above can be expressed in terms of elliptic integrals (4). They have also been tabulated (3).

The surface (Z = 0) displacements are

$$u_R^f(R, 0)/a = -\frac{p_0(1+\nu)(1-2\nu)}{2E} R, \quad R < 1 \tag{4a}$$

$$u_R^f(R, 0)/a = -\frac{p_0(1+\nu)(1-2\nu)}{2E} \frac{1}{R}, \quad R > 1 \tag{4b}$$

$$u_Z^f(R, 0)/a = \frac{4(1-\nu^2)p_0}{\pi E} E(R), \quad R < 1 \tag{4c}$$

$$u_Z^f(R, 0)/a = \frac{4(1-\nu^2)p_0}{\pi E} R\left[E\left(\frac{1}{R}\right) - \left(\frac{R^2-1}{R^2}\right) K\left(\frac{1}{R}\right)\right], \quad R > 1 \tag{4d}$$

where K(R) is the complete elliptic integral of the first kind and E(R) is the complete elliptic integral of the second kind.

The stress components along the centroidal axis (R = 0) are

$$\sigma_{RR}^f(0, Z)/p_0 = \sigma_{\theta\theta}^f(0, Z)/p_0 = \frac{1}{2}\left[ZI_0^2(0, Z) - (1+2\nu) I_0^1(0, Z)\right] \tag{5a}$$

$$\sigma_{ZZ}^f(0, Z)/p_0 = -I_0^1(0, Z) - ZI_0^2(0, Z) \tag{5b}$$

$$\sigma_{RZ}^f(0, Z)/p_0 = 0 \tag{5c}$$

where

$$I_0^1(0, Z) = 1 - \left(Z/\sqrt{1+Z^2}\right) \tag{5d}$$

$$I_0^2(0, Z) = 1/(1+Z^2)^{3/2} \tag{5e}$$

Adhesion Under a Flexibly Loaded Area

The adhesion problem is one in which there is no lateral displacement under the load while the surface outside the load is frictionless. These conditions are formulated for a uniform flexible loading as

$$\bar{\sigma}_{zz} = -p_0, \quad 0 \le r \le a, \quad z = 0 \tag{6a}$$

$$\bar{\sigma}_{zz} = 0, \quad r > a, \quad z = 0 \tag{6b}$$

$$\bar{u}_r = 0, \quad 0 \le r \le a, \quad z = 0 \tag{6c}$$

$$\bar{\sigma}_{rz} = 0, \quad r > a, \quad z = 0 \tag{6d}$$

It is noted that this case is identified by a bar over the appropriate stress or displacement component.

A solution to the elasticity problem with boundary conditions specified by Eqs. 6 is accomplished by use of the principle of superposition. The following boundary conditions specify a stress distribution:

$$\Delta\bar{\sigma}_{zz} = 0, \quad 0 \le r \le \infty, \quad z = 0 \tag{7a}$$

$$\Delta\bar{u}_r = -u_r^f = \frac{(1+\nu)(1-2\nu)}{2E} p_0 r, \quad 0 \le r \le a, \quad z = 0 \tag{7b}$$

$$\Delta\bar{\sigma}_{rz} = 0, \quad r > a, \quad z = 0 \tag{7c}$$

which when added to the frictionless solution will result in the solution to the boundary value problem specified by Eqs. 6.

A solution can be developed by integral transform methods (6). Applying Eq. 7a to the transformed stress function (ϕ^*) results in

$$\phi^* = -\frac{1}{\xi}\left[(1-2\nu) - \xi z\right] A_2 \exp(-\xi z) \tag{8}$$

The application of Eqs. 7b and 7c results in the dual integral equations,

$$\int_0^\infty \xi^2 A_2 J_1(\xi r) d\xi = \frac{1-2\nu}{4(1-\nu)} p_0 r, \quad r < a \tag{9a}$$

$$\int_0^\infty \xi^3 A_2 J_1(\xi r) d\xi = 0, \quad r > a \tag{9b}$$

General relationships for the solution of dual integral equations have been developed (2, 5). The coefficient (A_2) becomes

$$A_2 = 2\sqrt{2/\pi}\, A_1^1 \left[J_{3/2}(\lambda)/\lambda^{5/2}\right] \tag{10}$$

The transformed stress function (ϕ^*) is

$$\phi^* = \eta p_0 (\xi a)^{3/2} \left[(1-2\nu) - \xi z\right] \left[J_{3/2}(\xi a)/\xi^{7/2}\right] \exp(-\xi z) \tag{11a}$$

where

$$\eta = \frac{1-2\nu}{(1-\nu)\sqrt{2\pi}} \tag{11b}$$

The stress components are

$$\Delta\bar{\sigma}_{RR}/p_0 = -\eta\left[2K_0^1 - ZK_0^2 - \frac{2(1-\nu)}{R} K_1^0 + \frac{Z}{R} K_1^1\right] \tag{12a}$$

$$\Delta\bar{\sigma}_{\theta\theta}/p_0 = \eta\left[2\nu K_0^1 + \frac{2(1-\nu)}{R} K_1^0 - \frac{Z}{R} K_1^1\right] \tag{12b}$$

$$\Delta\bar{\sigma}_{ZZ}/p_0 = \eta Z K_0^2 \tag{12c}$$

$$\Delta\bar{\sigma}_{RZ}/p_0 = \eta \left[ZK_1^2 - K_1^1 \right] \tag{12d}$$

where

$$K_s^q = \int_0^\infty \lambda^{q-1/2} J_{3/2}(\lambda)\, J_s(R\lambda)\, \exp(-\lambda Z) d\lambda \tag{12e}$$

The stress components along the centroidal axis (R = 0) of the load are

$$\Delta\bar{\sigma}_{RR}(0, Z)/p_0 = \Delta\bar{\sigma}_{\theta\theta}(0, Z)/p_0 = \eta \left[(1 + \nu) K_0^1(0, Z) - \frac{Z}{2} K_0^2(0, Z) \right] \tag{13a}$$

$$\Delta\bar{\sigma}_{ZZ}(0, Z)/p_0 = \eta Z K_0^2(0, Z) \tag{13b}$$

$$\Delta\bar{\sigma}_{RZ}(0, Z)/p_0 = 0 \tag{13c}$$

where

$$K_0^1(0, Z) = \sqrt{2/\pi} \left[\tan^{-1}(1/Z) - Z/(1 + Z^2) \right] \tag{13d}$$

$$K_0^2(0, 2) = \sqrt{8/\pi}/(1 + 2^2)^2 \tag{13e}$$

The stress components due to adhesion are obtained by adding the above solution to the stress components due to the frictionless surface.

Figure 2 presents a profile of the radial and tangential stress along the centroidal axis. For an incompressible material ($\nu = 0.5$) there is no effect due to an adhesive surface. As the material becomes more compressible the radial stress, for both the frictionless and adhesive cases, decreases in magnitude. The magnitude of the decrease, in the adhesive case however, is substantially greater than for a frictionless surface.

A similar effect is shown in Figure 3, a profile of the vertical stress for both the adhesive and frictionless case. In the frictionless case the vertical stress is indpendent of Poisson's ratio. In the adhesive case, on the other hand, the vertical stress decreases with increasing compressibility. Near the surface the decrease is of the order of 25 percent. That is, a very compressible material will have a vertical stress some 25 percent less than an incompressible material.

The surface shear stress is

$$\bar{\sigma}_{RZ}(R, 0)/p_0 = -\frac{(1 - 2\nu)}{(1 - \nu)\pi} \frac{R}{\sqrt{1 - R^2}}, \quad R < 1 \tag{14a}$$

$$\bar{\sigma}_{RZ}(R, 0)/p_0 = 0, \quad R > 1 \tag{14b}$$

The lateral distribution of the surface shear stress is shown in Figure 4 for various values of Poisson's ratio (ν). For all but an incompressible material the shear stress starts at zero at the center and increases to infinity at the edges of the load. This is akin to the problem of a rigid load where the contact stresses are theoretically infinite at the edges of the load.

In a real material with adhesion the high shear stresses at the edges of the loaded area will induce some local yielding thus distributing frictional stresses along the surface. From a practical viewpoint the effect of tire loads on a pavement is to induce high shear stresses at the edges of the tire imprint.

The adhesive effect is directly opposed to the frictional effect. A frictional surface effect is one in which the magnitude of the shear stress is a maximum at the center of the load (R = 0) and dissipates to zero at the edge of the loaded area. In an adhesive condition the shear stress is zero at the center of the load. It increases to a maximum value at the edge of the loaded area.

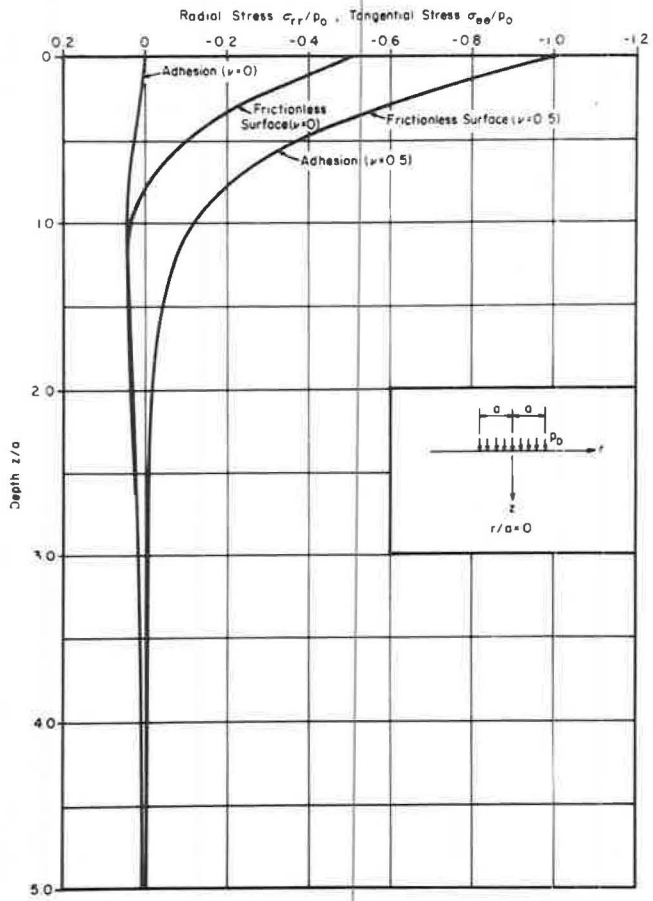

Figure 2. Radial and tangential stress profile—flexible load.

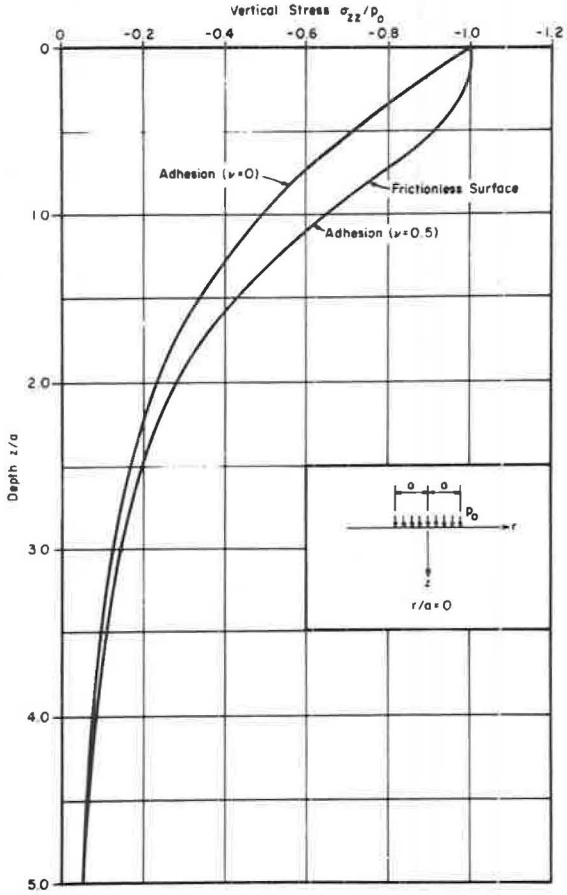

Figure 3. Vertical stress profile—flexible load.

It is also noted that if the material is incompressible the surface shear stress is zero. This confirms the fact that the frictional and adhesive solutions are identical for this special case.

The surface displacements are

$$\bar{u}_R(R, 0)/a = 0, \quad R < 1 \tag{15a}$$

$$\bar{u}_R(R, 0)/a = \frac{(1+\nu)(1-2\nu)}{E\sqrt{\pi}} p_0 \left[R \sin^{-1}(1/R) + \left(1 + \sqrt{R^2 - 1}\right)/R \right], \quad R > 1 \tag{15b}$$

$$\bar{u}_Z(R, 0)/a = \frac{1+\nu}{\pi E} p_0 \left[4(1-\nu) E(R) - \frac{(1-2\nu)^2}{1-\nu} \sqrt{1-R^2} \right], \quad R < 1 \tag{15c}$$

$$\bar{u}_Z(R, 0)/a = \frac{4(1-\nu^2)}{\pi E} p_0 R \left[E(1/R) - \frac{R^2 - 1}{R^2} K(1/R) \right], \quad R > 1 \tag{15d}$$

Figure 5 shows the lateral distribution of surface settlement. Adhesion under the load only affects the settlement under the load. Outside the loaded area the settlements are those of the frictionless case.

The effect of Poisson's ratio on the magnitude of settlement in the adhesive case is substantially different than in the frictionless case (Fig. 6). In the frictionless case the minimum surface settlement occurs for an incompressible material. As Poisson's ratio decreases the settlement decreases in magnitude

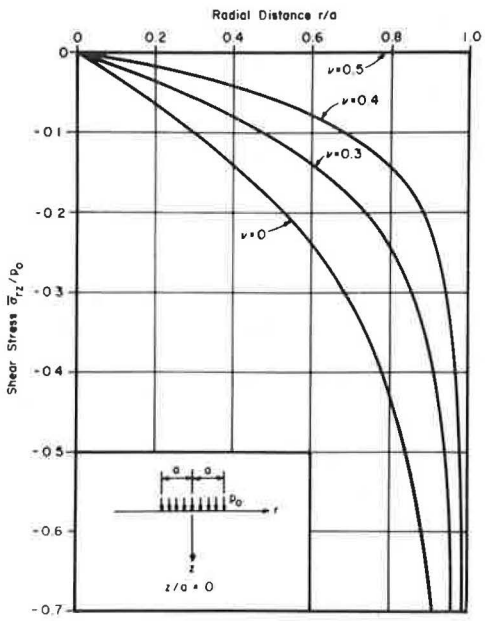

Figure 4. Radial distribution of surface shear stress—flexible load.

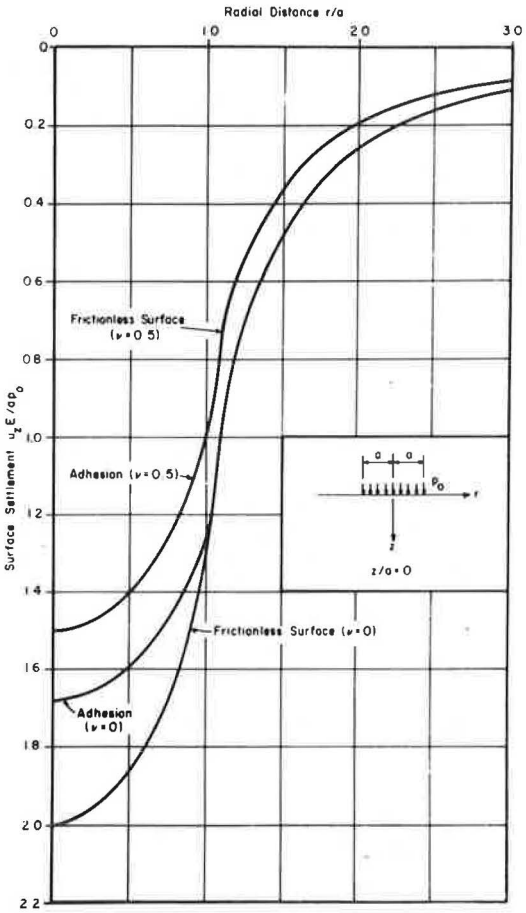

Figure 5. Surface settlement—flexible load.

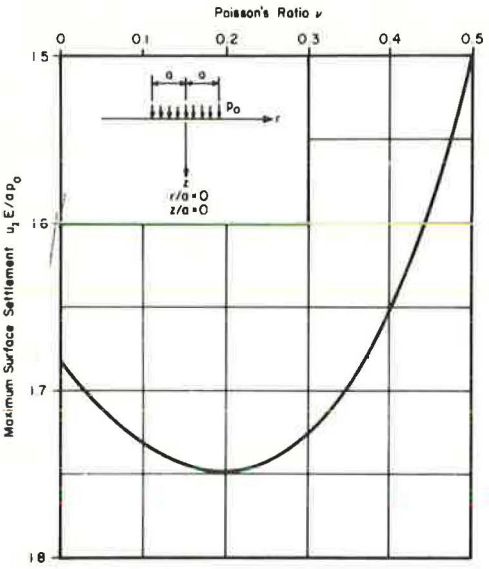

Figure 6. Effect of Poisson's ratio on maximum surface settlement—flexible load.

as an arithmetic progression. On the other hand, in the adhesive case the minimum settlement occurs at both ends (zero and one-half) of the Poisson ratio spectrum. The maximum settlement occurs in the neighborhood of (ν = 0.2). The settlement is about 14 percent higher than the minimum settlement.

Thus the effect of adhesion is to first reduce the overall magnitude of settlement. In addition, the effect of compressibility is substantially altered, in that the maximum settlement occurs for compressibilities which are approximately at a halfway point in the compressibility spectrum.

CONCLUSIONS

This paper has presented a solution for the stresses and displacements in an elastic half-space under the influence of surface adhesion. In addition to the numerical solutions presented there are several distinct features of surface adhesion.

The presence of adhesion reduces the magnitude of the stresses. The greatest stress reduction is in the lateral stresses.

For a frictionless surface the vertical stresses are independent of the elastic constants. The presence of adhesion implies a dependence on Poisson's ratio (ν).

The surface shear stress distribution produced by an adhesive surface starts at zero at the center of the load and goes to infinity at the edges of the load. This means that the friction induced by adhesion is greatest at the edges of the tire imprint on a pavement. Thus there are local shear failures along the perimeter of a flexible load.

ACKNOWLEDGMENTS

The work for this study was supported by the U. S. Bureau of Public Roads under Contract CPR-11-0989 with Rensselaer Polytechnic Institute.

REFERENCES

1. Boussinesq, J. Application de Potentiels a l'Etude de l'Equilibre et du Mouvement des Solides Elastiques. Gauthier-Villars, Paris, 1885.
2. Busbridge, I. W. Dual Integral Equations. Proc. London Mathematical Society, Vol. 44, No. 2, p. 115-129, 1938.
3. Eason, G., Noble, G., and Sneddon, I. N. On Certain Integrals of Lipshitz-Hankel Type Involving Products of Bessel Functions. Philosophical Trans., Royal Society, (A), Vol. 247, p. 529-551, London, 1955.
4. Love, A. E. H. The Stress Produced in a Semi-Infinite Solid by Pressure on Part of the Boundary. Philosophical Trans., Royal Society, (A), Vol. 228, p. 377-420, London, 1929.
5. Muki, R. Asymmetric Problems of the Theory of Elasticity for a Semi-Infinite Solid and a Thick Plate. Progress in Solid Mechanics. I. N. Sneddon and R. Hill, Eds. Vol. 1, p. 400-439, North-Holland Publishing Co., Amsterdam, 1960.
6. Sneddon, I. N. Fourier Transforms, McGraw-Hill, 1951.

Stresses and Displacements in Viscoelastic Pavement Systems Under a Moving Load

Y. T. CHOU, U. S. Army Engineer Waterways Experiment Station, and
H. G. LAREW, University of Virginia

The design of flexible pavements requires a knowledge of the stresses and displacements induced by traffic. This paper is a study of the response of viscoelastic materials to moving loads in pavement systems. By neglecting the inertia effect, expressions for stresses and displacements in single- and two-layered viscoelastic systems are developed for a moving concentrated load based on the elastic-viscoelastic correspondence principle. Numerical solutions for various types of materials at various speeds of the load and discussions of the influence and relative importance of various factors affecting the solutions are presented. Comparisons are made between existing field measurements of stress and displacement and the results obtained in this study. The computed stresses and displacements decrease with increasing speed of the load as well as with increasing value of retardation time of the viscoelastic material. For viscous materials, the displacements continue to increase as the load moves away from the station, but the maximum stress always occurs when the load is directly over the station. The stresses and displacements in the subgrade soils are reduced when a reinforcing layer is present. The degree of reduction depends on the speed of the load and the relative material properties for each layer.

•IN recent years, there has been an increasing interest in the application of dynamic theory to the structural design of pavements. Although engineers realize that a highway pavement is subject to moving loads as well as stationary ones, most current methods of pavement design are based on the assumptions that the pavement materials are time-independent and linearly elastic, and that the design wheel load is stationary. Since highway pavement materials have both elastic and viscous properties (1), the stress-strain relations for the materials are not constant but vary with time. Recent research has shown that, under small strains, asphalt mixtures exhibit viscoelastic behavior (2) and that a viscoelastic theory should give a better approximation of the displacements in pavement systems than that obtained by elastic theories (3). Space technology has also advanced in recent years as a result of studies of the viscoelastic behavior of solid rocket propellants (4, 5).

The analysis of linear viscoelastic media is generally based on the correspondence principle developed by Lee (6), which permits the application of existing elastic theory to the solution of the viscoelastic problem. Considerable work, based on this principle, has been done in the analysis of both elastic and viscoelastic plates on viscoelastic foundations (7). The application of the principle to the analysis of layered systems was initiated by Ishihara (8) and Westmann (9) in 1962.

Paper sponsored by Committee on Strength and Deformation Characteristics of Pavement Sections and presented at the 48th Annual Meeting.

The analysis of viscoelastic pavements subjected to moving loads has received increasing attention. One approach (10, 11, 12) considers the pavement to be a viscoelastic beam or plate supported by a linearly elastic foundation. This beam or plate is loaded by a concentrated force moving at constant velocity. Perloff and Moavenzadeh reported (13) a thorough study of the surface deflection characteristics of a viscoelastic medium under a moving point load. They found that the response of pavement materials to moving loads was quite different from the response to stationary loads.

The study reported herein expands Perloff's and Moavenzadeh's work to layered systems. Information is presented that may lead to a better understanding of the influence and relative importance of the various factors that enter the problem, i.e., material properties and the speed of moving loads. A method of analysis was developed and, by neglecting inertia forces, equations were derived for stresses and displacements induced by moving concentrated loads at points on and below the surface of viscoelastic pavement systems. The equations were solved on a digital computer.

In deriving equations for layered systems, a "rough" interface was assumed, i.e., the displacement in the horizontal direction and the shearing stress were continuous across the interface. It was felt that a rough interface would better describe the actual condition of flexible pavement structures.

To show the effect of a reinforcing layer on the reduction of stresses and displacements at the subgrade soils, computations were included for viscoelastic semi-infinite solids that had the same material properties as the subgrade soils. These computations were compared with those for layered systems. Because the stresses and displacements under moving loads decrease rapidly with increasing speed of the load, numerical solutions were obtained for various speeds and several types of materials. These results were then compared with solutions for stationary loads.

It was felt that a dimensional presentation of several variables could best serve one essential purpose of this study, i.e., to show the effect of the speed of the load and the variations of material properties on the stresses and displacements in pavement systems. Therefore, time, t, was expressed as seconds and velocity, v, as miles per hour in the numerical presentations.

Since layered systems were difficult to analyze, even with a high-speed digital computer, an incompressible material and a Kelvin model were assumed for each layer to describe the behavior of the linear viscoelastic materials. To obtain compatible results the same were assumed in single-layer systems. The results presented herein are limited to one- and two-layer systems.

ELASTIC ANALYSIS

Single-Layer Systems

The expressions for vertical stresses and vertical displacements (in the remainder of the discussion, stress and displacements are considered to be "vertical") in a semi-infinite elastic half space, subjected to a vertical normal load, can be found in Timoshenko and Goodier (14):

$$S_Z = -\frac{3q_0}{2\pi} Z^3 (R^2 + Z^2)^{-5/2} \tag{1a}$$

$$W = \frac{q_0}{2\pi E}\left[(1+\nu^2)(R^2+Z^2)^{-3/2} + 2(1-\nu^2)(R^2+Z^2)^{-1/2}\right] \tag{1b}$$

where

ν = Poisson's ratio,
E = Young's modulus,
R = horizontal distance from the normal load to the point where the stress and displacement are found, and
Z = depth of the point from the surface.

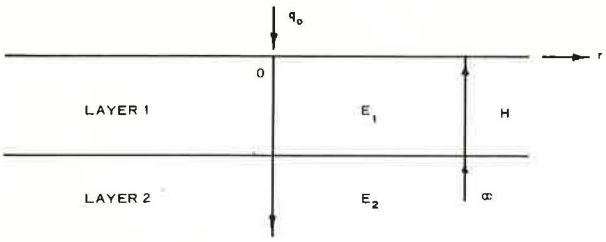

Figure 1. A two-layer elastic system.

Two-Layer System

The elastic solution for two- and three-layer systems was developed by Burmister (15), and later extended by Mehta and Veletsos (16), by using stress function method to determine the components of stress and displacement under stationary loads.

A two-layer elastic system is shown in Figure 1. The Young's moduli of layers 1 and 2 are E_1 and E_2, respectively, and the Poisson's ratio for each layer is assumed to be one-half. Eqs. 2 express the displacement W_0 on the surface, and the displacement W_1 and the stress σ_1 at a point 2H below the surface of a two-layer system under a normal point load, q_0. The derivation of the equations can be found elsewhere (16, 17).

$$W_0 = \frac{1}{4\pi H^2} \int_0^\infty J_0 (m\rho)\, V_0\, dm \tag{2a}$$

$$W_1 = \frac{1}{4\pi H^2} \int_0^\infty J_0 (m\rho)\, V_1\, dm \tag{2b}$$

$$\sigma_1 = -\frac{1}{2\pi H^2} \int_0^\infty m\, J_0 (m\rho)\, V\, dm \tag{2c}$$

where

J_0 = Bessel function of the first kind and order zero,
m = a parameter
$\rho = R/H$,

$$V_0 = \frac{3q_0}{E_1} \frac{1 + 4Nme^{-2m} - N^2e^{-4m}}{1 - 2N(1 + 2m^2)\, e^{-2m} + N^2e^{-4m}},$$

$$V_1 = \frac{3q_0}{E_2} (1 - N) \frac{(1 + 2m)\, e^{-2m} - N(1 - 2m^2)\, e^{-4m}}{1 - 2N(1 + 2m^2)\, e^{-2m} + N^2e^{-4m}},$$

$$V = q_0(1 - N) \frac{(1 + 2m)\, e^{-2m} - N(1 - 2m^2)\, e^{-4m}}{1 - 2N(1 + 2m^2)\, e^{-2m} + N^2e^{-4m}}, \text{ and}$$

$$N = \frac{E_1 - E_2}{E_1 - E_2}.$$

Moving Load

Since the speeds of the vehicle loads traveling on highway pavement are much less than the speeds of the shear and compression waves propagated in the pavement structures, it was assumed that inertial effects are negligible. The problem was therefore treated as quasi-static.

The pavement structure was assumed to be at rest initially. For times greater than zero, the surface of the pavement was subjected to a concentrated load of magnitude,

q_o, moving along the r-axis with constant speed, v (Fig. 1). The elastic problem for a q_o loading at a given instant is solved by Eqs. 1 and 2 by shifting the origin of coordinates. R can be represented as

$$R = \left| R_o - vt \right|$$

where R_o is the horizontal distance from the origin, o, to the point where the stress and displacement are sought. In this study, o corresponds to the initial position of the moving load.

VISCOELASTIC ANALYSIS

Material Characterization

The viscoelastic stress-strain relations used throughout this paper are based on the principle of elastic-viscoelastic correspondence developed by Lee (6) and are defined by means of linear differential operators with respect to time. For a linear, homogeneous, and isotropic material, the stress-strain relation can be represented by two pairs of operators, one of which relates the deviatoric (shearing) stress to the deviatoric strain, the other the mean normal dilatational (volumetric) stress to the mean normal strain. For an incompressible material, the bulk modulus of the material, K, becomes infinite. Attention was concentrated on the shearing stress and shearing strain relations.

The behavior of a viscoelastic material in pure shear is represented by a differential relation in the form

$$P\, s_{ij} = 2Q e_{ij} \tag{3}$$

where

s_{ij} = deviatoric stress = $\sigma_{ij} - \left(\frac{1}{3}\right) \delta_{ij}\, \sigma_{kk}$,

e_{ij} = deviatoric strain = $\epsilon_{ij} - \left(\frac{1}{3}\right) \delta_{ij}\, \epsilon_{kk}$,

σ_{ij} = stress tensors,

ϵ_{ij} = strain tensors,

δ_{ij} = Kronecker delta (i.e., $\delta_{ij} = 1$ when $i = j$; $\delta_{ij} = 0$ when $i \neq j$),

$$P = \sum_{r=0}^{m} a_r \frac{\partial^r}{\partial t^r}, \text{ and}$$

$$Q = \sum_{r=0}^{n} a_r \frac{\partial^r}{\partial t^r}.$$

The analogous equation for the elastic solid is

$$s_{ij} = 2\, G\, e_{ij} \tag{4}$$

where G is the shear modulus.

Compare Eqs. 3 and 4:

$$G = \frac{Q}{P} = \sum_{r=0}^{n} a_r \frac{\partial^r}{\partial t^r} \Bigg/ \sum_{r=0}^{m} a_r \frac{\partial^r}{\partial t^r} \tag{5}$$

For incompressible materials, Young's modulus, E, and Poisson's ratio, ν, are related to G and K.

$$E = 9KG/(3K + G) = 3G \tag{6a}$$

$$\nu = (3K - 2G)/(6K + 2G) = 0.5 \tag{6b}$$

To eliminate the time variable, the Laplace transform with respect to t can be applied to Eq. 3. The transforms of stresses and strains are denoted by a star on the corresponding function. If the system is initially undisturbed, i.e., with initial stress and strain conditions equal to zero, an operator in $\frac{\partial}{\partial t}$ merely becomes the same function of the transformed variable p, so Eq. 3 becomes

$$P(p)s_{ij}^{*} = 2Q(p)e_{ij}^{*} \tag{7}$$

where

$$P(p) = \sum_{r=0}^{m} a_r p^r$$

and

$$Q(p) = \sum_{r=0}^{n} a_r p^r$$

If the Laplace transforms of the stresses and strains are considered, and if G^* is defined as follows

$$G^{*} = \frac{s_{ij}^{*}}{2e_{ij}^{*}} = \frac{Q(p)}{P(p)} \tag{8}$$

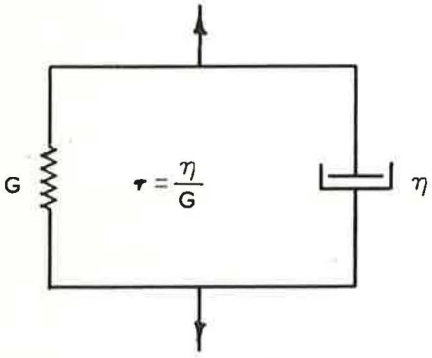

Figure 2. Kelvin model representing response to deviatoric stress.

then by replacing G and q_0 in the elastic equations for stresses and displacements with G^* and q_0^*, respectively, the equations for the Laplace transforms of stresses and displacements are obtained. These equations are functions of the transformed variable, p, and their inversions give the stresses and displacements in terms of t.

If it is assumed that the response of the material to deviatoric stress can be represented by a Kelvin model, and that the response of the material to mean normal stress is infinitely rigid ($K = \infty$) as shown in Figure 2, the transformed shear modulus of the Kelvin material is

$$G^{*} = G + \eta p = G(1 + \tau p) \tag{9}$$

where τ is the retardation time.

From Eqs. 6a and 9, the transformed Young's modulus E^* becomes

$$E^{*} = 3G(1 + \tau p) \tag{10}$$

Single-Layer Systems

For a single-layer incompressible system, the associated elastic problem for the displacement has the form

$$W^* = \frac{3}{4\pi E^*}\left\{q_0 Z^2\left[(R_0 - vt)^2 + Z^2\right]^{-3/2} + q_0\left[(R_0 - vt)^2 + Z^2\right]^{-1/2}\right\}^* \qquad (11)$$

The viscoelastic solution can be obtained readily by using the convolution integral (18). Substituting Eq. 10 into Eq. 11 and applying the convolution theorem gives

$$W = \frac{4\pi}{q_0} GW(t) = \int_0^t \frac{1}{\tau}\exp\left(-\frac{t-\tau'}{\tau}\right)\left\{Z^2\left[(R_0 - v\tau')^2 + Z^2\right]^{-3/2} + \left[(R_0 - v\tau')^2 + Z^2\right]^{-1/2}\right\} d\tau' \qquad (12)$$

where τ' is a time variable varying from zero to t.

Eq. 12 was integrated numerically on the Burroughs B-5500 digital computer by use of Simpson's rule. For displacements on the surface, the method used by Perloff and Moavenzadeh (13) also was used to avoid the singularity. In this method the conditions where the load approaches the point and the conditions where it moves away from the point are considered separately. Eq. 12 can be written as

$$W = \int_0^{\frac{R_0}{v}(1-\epsilon)} \frac{1}{\tau(|R_0 - v\tau'|)}\exp\left(-\frac{t-\tau'}{\tau}\right)d\tau' + \int_{\frac{R_0}{v}(1+\epsilon)}^{t} \frac{1}{\tau(|R_0 - v\tau'|)}\exp\left(-\frac{t-\tau'}{\tau}\right)d\tau' \qquad (13)$$

where ϵ is any positive number less than unity.

Two-Layer Systems

The method employed for solving two-layer viscoelastic systems is applicable when the equations for stress and displacement can be reduced to a form suitable for direct Laplace inversion. These equations for stresses and displacements in the transformed domain for a two-layer elastic system and a moving concentrated load are

$$W_0^* = \frac{1}{4\pi H^2}\int_0^\infty \left\{q_0 J_0\left[m(\rho - Vt)\right]\right\}^* V_0^*\, dm \qquad (14a)$$

$$W_B^* = \frac{1}{4\pi H^2}\int_0^\infty \left\{q_0 J_0\left[m(\rho - Vt)\right]\right\}^* V_B^*\, dm \qquad (14b)$$

$$\sigma_B^* = \frac{-1}{2\pi H^2} \int_0^\infty \left\{ m q_0 J_0 \left[m(\rho - Vt) \right] \right\}^* V_\sigma^* \, dm \tag{14c}$$

where

$$V = \frac{v}{H},$$

$$\sigma = \frac{R_0}{H},$$

and V_0^*, V_B^*, V_σ^* are the same as shown in Eqs. 2 except that N, G_1, and G_2 are replaced by N^*, G_1^*, and G_2^*.

Moreover, the viscoelastic solution for two-layer systems can be obtained by using convolution integral, as in the case of single-layer systems. After the exchange of integrals, we have

$$W_0 = \frac{4\pi}{q_0} W_0(t) = \frac{1}{H^2} \int_0^t \int_0^\infty J_0 \left[m(\rho - V\tau') \right] V_0(t - \tau') \, dm d\tau' \tag{15a}$$

$$W_B = \frac{4\pi}{q_0} W_B(t) = \frac{1}{H^2} \int_0^t \int_0^\infty J_0 \left[m(\rho - V\tau') \right] V_B(t - \tau') \, dm d\tau' \tag{15b}$$

$$\sigma_B = -\frac{2\pi}{q_0} \sigma_B(t) = \frac{1}{H^2} \int_0^t \int_0^\infty m J_0 \left[m(\rho - V\tau') \right] V_\sigma(t - \tau') \, dm d\tau' \tag{15c}$$

where τ' is a time variable varying from zero to t, and the expression $(t - \tau')$ means that V_0, V_B, and V_σ are functions of $(t - \tau')$.

Mathematically, the exchange of integrals is possible because the inner integrals of Eqs. 15 are uniformly convergent in the range $0 \leq \tau' \leq t$ (19). This exchange is desirable since it greatly reduces the computation time.

Assume that the incompressible materials in layers 1 and 2 of a two-layer system are characterized by the models shown in Figure 2. From Eqs. 2, 9, and 10, let $\tau_{12} = \tau_1/\tau_2$, $G_{12} = G_1/G_2$, and p = the transformed variable of time, t. Then the Laplace transformations of V_0, V_B, and V_σ can be obtained:

$$V_0^* = \frac{1}{G_2 G_{12} \tau_{12} F_0} \frac{A_0 p^2 + B_0 p + C_0}{(\tau_1 p + 1)(p^2 + D_0 p + E_0)} \tag{16a}$$

$$V_B^* = \frac{2}{G_2 F_0} \frac{B_1 p + C_1}{p^2 + D_0 p + E_0} \tag{16b}$$

$$V_\sigma^* = \frac{2}{F_0} \frac{B_1 \tau_2 p^2 + (B_1 + C_1 \tau_2) p + C_1}{p^2 + D_0 p + E_0} \tag{16c}$$

where

$$A_0 = (G_{12}\tau_{12} + 1)^2 + 4me^{-2m}(G_{12}^2 \tau_{12}^2 - 1) - e^{-4m}(G_{12}\tau_{12} - 1)^2$$

$$B_0 = 2\left[(G_{12} + 1)(G_{12}\tau_{12} + 1) + 4me^{-2m}(G_{12}^2 \tau_{12} - 1) - e^{-4m}(G_{12} - 1)(G_{12}\tau_{12} - 1) \right]$$

$$C_0 = (G_{12} + 1)^2 + 4me^{-2m}(G_{12}^2 - 1) - e^{-4m}(G_{12} - 1)^2$$

$$F_0 = (G_{12}\tau_{12} + 1)^2 - 2(1 + 2m^2)e^{-2m}(G_{12}^2\tau_{12}^2 - 1) + e^{-4m}(G_{12}\tau_{12} - 1)^2$$

$$D_0 = \frac{2}{F} \cdot \left[(G_{12} + 1)(G_{12}\tau_{12} + 1) - 2(1 + 2m^2)e^{-2m}(G_{12}^2\tau_{12} - 1) + e^{-4m}(G_{12} - 1)(G_{12}\tau_{12} - 1)\right]$$

$$E_0 = \frac{1}{F} \cdot \left[(G_{12} + 1)^2 - 2(1 + 2m^2)e^{-2m}(G_{12}^2 - 1) + e^{-4m}(G_{12} - 1)^2\right]$$

$$B_1 = (G_{12}\tau_{12} + 1)(1 + 2m)e^{-2m} - (G_{12}\tau_{12} - 1)(1 - 2m^2)e^{-4m}$$

$$C_1 = (G_{12} + 1)(1 + 2m)e^{-2m} - (G_{12} - 1)(1 - 2m^2)e^{-4m}$$

The values of V_0, V_B, and V_σ in Eqs. 15 can be obtained by inverting Eqs. 16. To solve the double integral in Eqs. 15, the inner integral was evaluated by the use of the Gaussian quadrature formula; the outer integral by Simpson's rule. The singularity that exists in Eq. 15a for the surface displacement was treated in a manner similar to that employed in the case of a single layer.

For systems of more than two layers or for compressible material, the mathematical work required for the direct inversion method becomes very tedious, and the polynomial that results is of such a high degree that its roots are almost impossible to find. Therefore, the direct inversion method is used mainly when stress and displacement equations can be reduced to a sum of simple partial fractions. For multi-layer or compressible material, the collocation inversion method originally proposed by Schapery (20) should be used. This method was successfully employed by Huang (21) for analyzing four-layer compressible systems under stationary loads. Moreover in the present study, it was found that the collocation method also was applicable for moving loads. However, the results obtained for multi-layer systems by the collocation method were limited in this study because of the excessive computer time required. The results for multi-layer systems and the theory of the collocation method can be found elsewhere (17).

PRESENTATION AND DISCUSSION OF NUMERICAL RESULTS

Eqs. 12 and 15 were used to compute the stresses and displacements at selected points in pavement systems. In so doing, numerical values were assigned to the variables H, ρ, V, and t. H, the thickness of the top layer, was assumed to be 1 ft. In the case of the single-layer system, the stresses and displacements were computed at a point 2 ft below the surface. For comparison, it was assumed that the material properties in the lower layer of the two-layer systems were the same as those in the single-layer system. The effect of a reinforcing layer in reducing the stress and displacement in the subgrade soils could thus be studied. The dimensionless factor ρ or R_0/H cannot be factored out of the Bessel function $J_0[m(\rho - V\tau')]$ as in the case of the load q_0; therefore, a numerical value was assigned to ρ. In the expression for ρ, R_0 is the horizontal distance from the starting point of the load to the point where the stresses and displacements are to be determined. The traveling time, for a given value of R_0, varied with the value of v. It was clear that for large values of v, greater values of R_0 should be provided. However, when a very large value of R_0 was used, the upper limit of integration was increased. Moreover, the error term for Simpson's rule integration is a function of the fifth degree of interval size. Hence, the proper value of R_0 was chosen so that the calculated displacements did not change significantly when greater values of R_0 were used. To find the proper value of R_0, a series of values of t equal to 10,000 sec, 1,000 sec, 100 sec, and 10 sec was assigned to Eq. 12 to compute the displacements. For this case R_0 was replaced by the expression vt, and as a result, a value of R_0 equal to 100 v was determined most suitable for use in the subsequent numerical computations

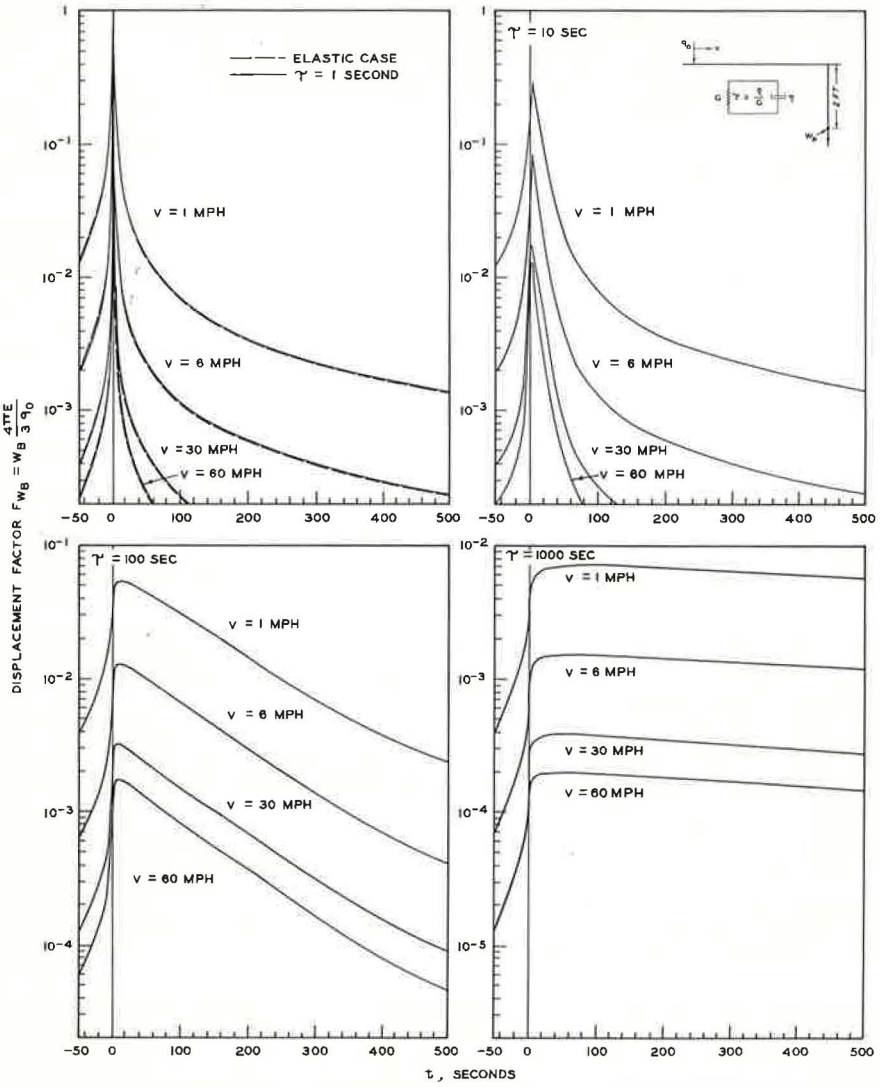

Figure 3. Effect of speeds on displacement factors 2 ft below surface—single-layer incompressible systems.

in this study. In Eqs. 15, V stands for v/H, where v is the speed of the moving load; t is the time the load traveled from its initial position. It should be noted that both stress and displacement increased if a value of R_0 greater than 100 v was used. This effect was more pronounced when the material became more viscous.

Single-Layer Systems

The effect of speed of the moving load on the displacements at a point 2 ft below the surface of a single-layer system at four different values of retardation time is shown in Figure 3. The retardation time τ is defined as the ratio of the viscosity to the spring modulus of the model. For convenience of presentation, the time was set at zero when the load was directly over the station where the displacements were to be computed.

As the speed of the load increases, the displacement decreases (Fig. 3). This is not surprising, since higher speed implies a shorter time during which the considered point

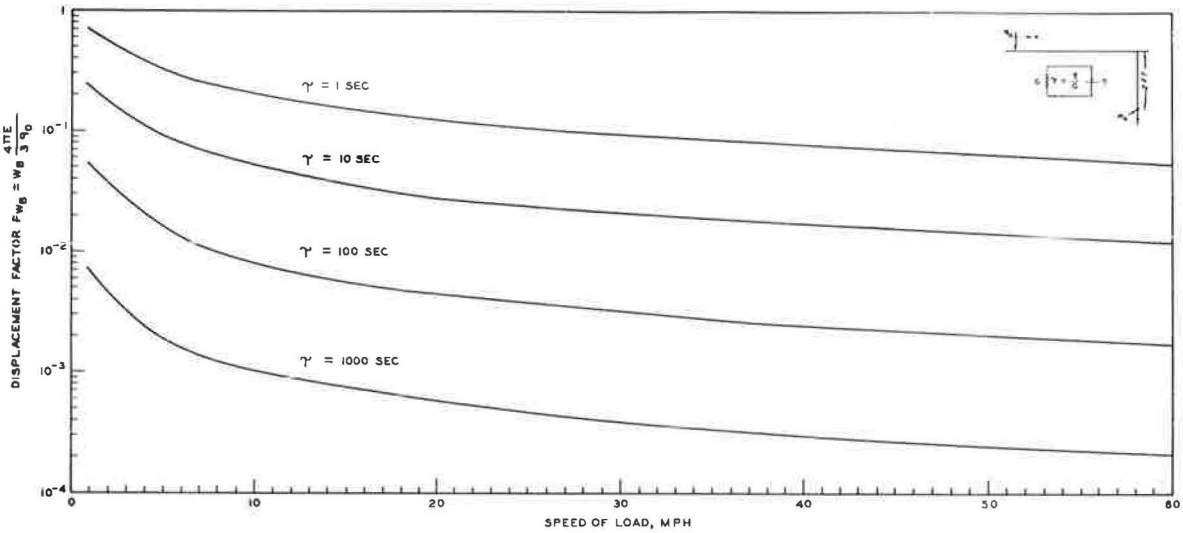

Figure 4. Effect of speeds on displacement factors 2 ft below surface—single-layer incompressible systems.

is subjected to a given stress. Moreover, a large value of retardation time implies a lower rate of deformation in the viscoelastic material and, consequently, a smaller displacement for a given time.

As the load approaches the station, the relations of various velocities to a given retardation time are quite similar (Fig. 3), but displacement generally increases as the velocity decreases. Moreover the rebound displacement, as measured by F_{W_B}, occurs more quickly for smaller retardation times.

For comparison, solutions for the perfectly elastic case were plotted as dashed lines (Fig. 3) with the curves for τ = 1 sec. For a short retardation time, τ = 1 sec, the elastic and viscoelastic solutions are almost the same. The comparisons are based on a constant value of spring modulus, G, for the model. For two different materials having the same retardation time, however, one can have a greater shear modulus than the other.

To determine the variation of the displacements at unusually low and high speeds, relations were also computed using speeds of 0.1, 120, 200, 300, and 400 mph. The shapes of the displacement curves at these speeds were quite similar to those in Figure 3 and are not presented here. It should be pointed out, however, that as the speed of the moving load increases, the inertia effect becomes more significant, and the method of computation used here does not yield correct results.

The effects of speed of the moving load on the maximum displacements at various values of retardation time are shown in Figure 4. The maximum displacement decreased as v and τ increased. When the maximum displacements at a point 2 ft below the surface for v = 60 mph were compared with those under a stationary load, the ratios were 5.57×10^{-2}, 1.23×10^{-2}, 1.17×10^{-3}, and 2.1×10^{-4} for τ = 1, 10, 100, and 1000 sec, respectively.

Two-Layer Systems

The general behavior of the displacements in two-layer systems was rather similar to that of single-layer systems. Displacement-time curves for a point 2 ft below the surface for τ_{12} equals 10 and 0.5, respectively, are shown in Figure 5. The shapes of the curves are very similar to those for the single layer, except the displacements are reduced because of the upper reinforcing layer. In view of this, the shape of the curves for multi-layer systems is also believed to be similar to that for single-layer systems. The displacement decreased with increasing value of the ratio τ_{12} for lower speeds, if the material in the bottom layer was very viscous.

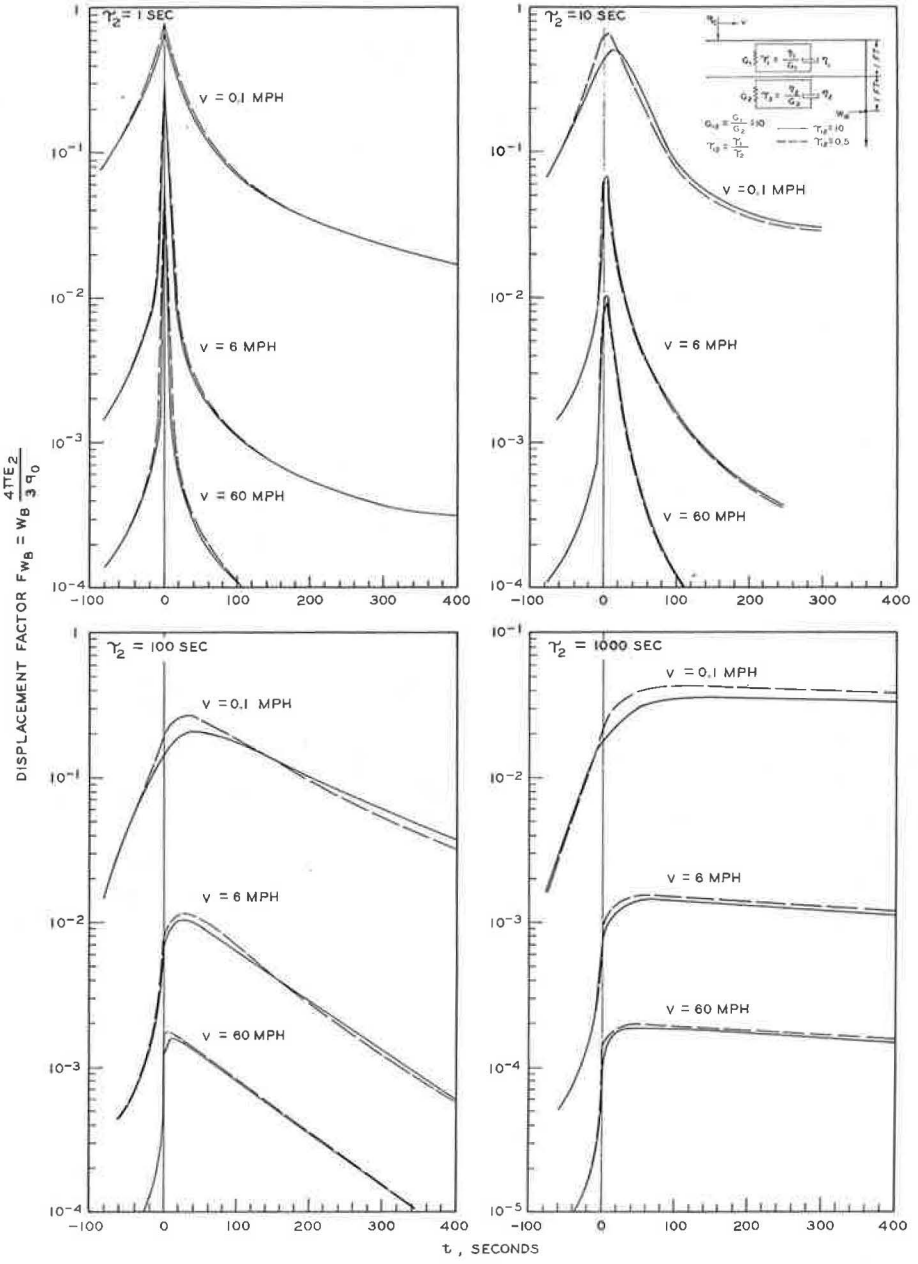

Figure 5. Effect of speeds on displacement factors 2 ft below surface—two-layer incompressible systems.

Since a reinforcing layer is placed on the subgrade soil to reduce the stress and displacement in the subgrade soil, the ratios of the displacements for single- and two-layer systems for various v, τ_2, and τ_{12} values were computed (Table 1). For v = 0.1 and 1 mph, and for τ = 1 sec, the displacement decreased appreciably because of the reinforcing layer, even when τ_{12} was less than unity. For $\tau_2 \geq 100$ sec, the displacement decreased only slightly when $\tau_{12} < 1$, but decreased appreciably when $\tau_{12} = 10$. For all values of τ_{12}, the effect of reinforcing layer decreased as the value of τ_2 increased. To reduce the subgrade soil displacements under very slow moving vehicle loads or parked vehicles, the following suggestions should be followed:

TABLE 1

EFFECT OF REINFORCING LAYER IN REDUCING SUBGRADE DISPLACEMENT—TWO-LAYER SYSTEMS

v (mph)	τ_2 (sec)	Ratio of Displacement in Two-Layer Systems to Single-Layer Systems (G_{10} = 10)		
		τ_{12} = 0.5	τ_{12} = 1.0	τ_{12} = 10
0.1	1	0.74	0.73	0.68
	10	0.83	0.80	0.71
	100	0.95	0.92	0.74
	1000	0.97	0.94	0.82
1.0	1	0.87	0.83	0.70
	10	0.90	0.86	0.74
	100	0.96	0.94	0.84
	1000	0.98	0.96	0.88
6.0	1	0.95	0.90	0.73
	10	0.96	0.92	0.76
	100	0.96	0.94	0.85
	1000	0.98	0.96	0.89
60.0	1	0.97	0.92	0.84
	10	0.97	0.94	0.87
	100	0.98	0.95	0.90
	1000	0.98	0.97	0.94

1. For elastic subgrades, construction of a reinforcing layer that is stiffer than the subgrade soil is most beneficial. The displacement can be decreased further if the value of τ_{12} is greater than unity.
2. For viscous subgrades, the capacity for retarding displacement in the reinforcing layer should be larger than that for the subgrade, i.e., τ_{12} should be greater than unity; otherwise a stiff reinforcing layer is of little valuc.

When loading speed was increased to 6 mph, the influence of the reinforcing layer was not significant for the case τ_2 = 1 sec, unless τ_{12} was greater than unity. A similar influence of the reinforcing layer also was observed in the case where the subgrade be-

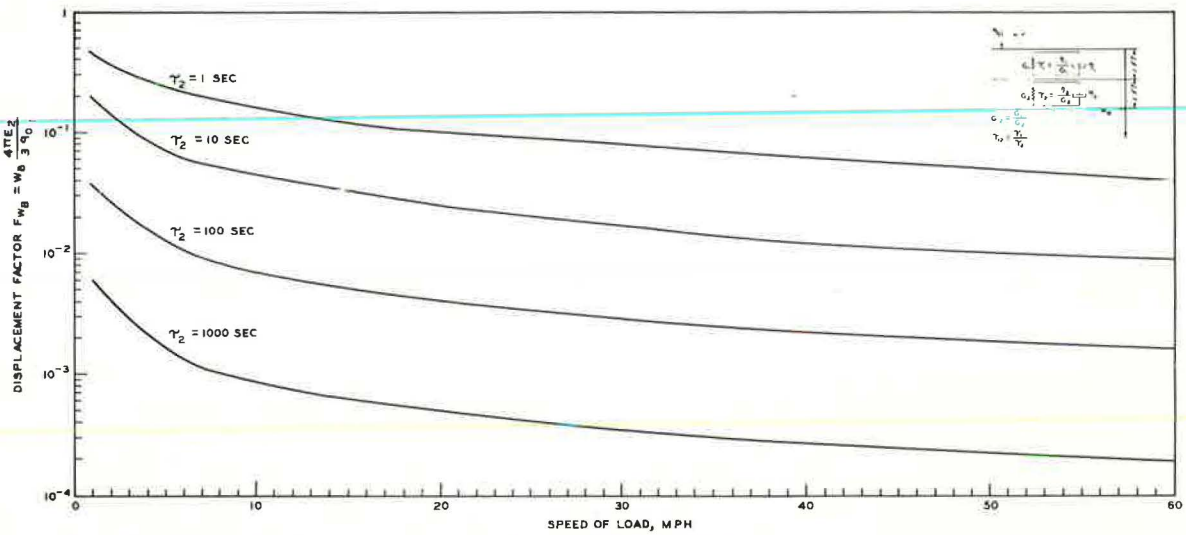

Figure 6. Effect of speeds on displacement factors 2 ft below surface—two-layer incompressible systems ($G_{10} = \tau_{12} = 10$).

TABLE 2

STRESS FACTOR AS A FUNCTION OF t, τ_2, AND v

Incompressible Two-Layer System—2 Ft Below Surface ($G_{12} = \tau_{12} = 10$) The Tabulated Values Represent the Quantity $-\sigma_Z \frac{2\pi}{q_o}$										
v = 1, mph	t	20	40	70	90	100	125	150	175	200
	$\tau_2 = 1$	-6.03 at -5	-4.77 at -5	-1.85 at -5	-1.79 at -4	1.85 at -1	5.93 at -4	-1.21 at -6	9.3 at -5	7.53 at -4
	t	20	40	70	90	100	125	150	175	200
	$\tau_2 = 10$	-1.72 at -5	-2.54 at -5	-2.72 at -5	-3.32 at -4	1.36 at -1	5.38 at -3	2.54 at -3	0.38 at -4	-0.78 at -6
	t	20	40	70	90	100	102	110	150	200
	$\tau_2 = 100$	-1.67 at -6	-3.76 at -6	-8.61 at -6	-3.71 at -4	1.29 at -1	6.22 at -2	8.90 at -4	1.15 at -3	1.76 at -3
	t	20	40	70	90	100	102	110	150	200
	$\tau_2 = 1000$	1.53 at -7	-7.86 at -7	-5.11 at -6	-3.75 at -4	1.28 at -1	6.09 at -2	-2.33 at -4	1.43 at -4	9.63 at -4

came more viscous, i.e., as τ_2 of the bottom layer increased. When v was further increased to 60 mph, the significance of the reinforcing layer was practically unnoticeable.

It is concluded that the effect of a reinforcing layer in reducing the displacements in the bottom layer increased with increasing values of τ_{12}, but decreased with increasing speeds of the load, as well as increasing values of the retardation time of the material in the bottom layer.

Because Perloff and Moavenzadeh (13) thoroughly discussed the surface deflection characteristics of a viscoelastic compressible medium under a moving point load, the results for surface displacements are not presented herein. However, the surface displacement curves were very similar to those obtained for displacements 2 ft below the surface.

The effect of speed of load on displacement in two-layer systems at a point 2 ft below the surface is shown in Figure 6. The displacement decreased with increasing speed of the load and with increasing value of the retardation time of the bottom layer.

The values of the stress factor, S_B, are shown in Table 2 for different times in the viscoelastic system under a moving point load. Because very long computer time was needed to obtain accurate results as v was increased, the numerical solutions at different times presented are only for a v of 1 mph. The maximum stress (for this case, compression) always occurred at the time when the load was directly over the station. When the load moved toward or away from the station, the stresses changed signs.

The relation between the stress factor S_B and the speed of the load is shown in Figure 7 for four values of τ_2. The stress factor decreased with increasing v and then reached a constant value as v exceeded 15 mph.

Considerable computer time was required to obtain accurate results for two-layer systems. The main difficulty developed in evaluating the outer integral in Eqs. 15 by Simpson's rule. Not only did the values of the inner integral vary irregularly with the values of τ', but the expressions for V_0, V_B, and V_σ were very complicated. The degree of complexity of the function to be integrated depended upon the speed of the load, material properties, and time (or loading position). For a given material property, the computer time generally increased with increasing speed of the load and with increasing value of the upper limit in the Simpson's integration. However, for given values of v and t, the variation of computer times with material properties was irregular. In some cases, the computer time changed greatly with a change of only one variable of the material properties, i.e., τ_{12}, G_{12}, and τ_2. In several cases, a solution required more than 60 min on the Burroughs B-5500 digital computer.

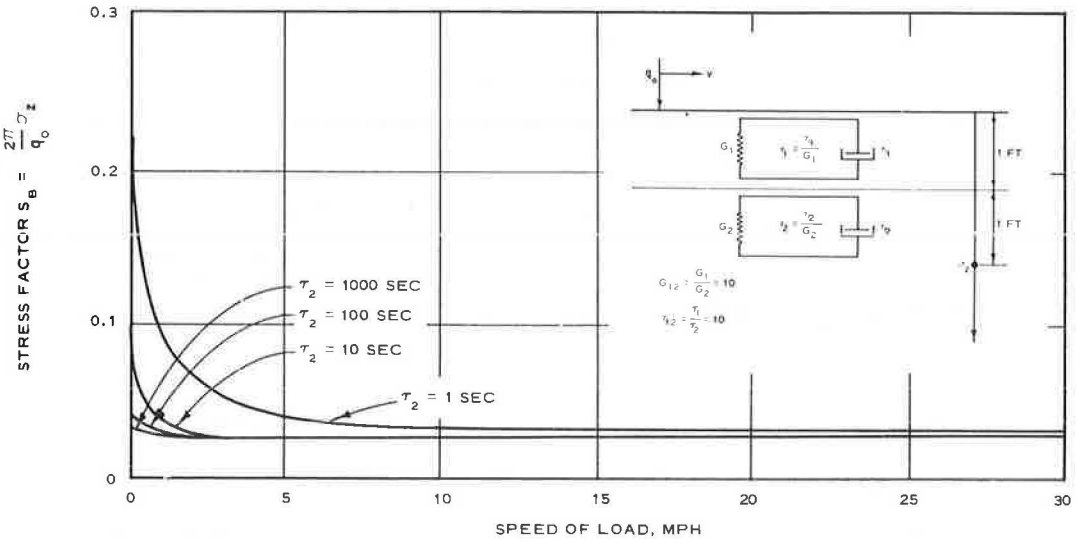

Figure 7. Effect of speeds on stress factors 2 ft below surface—two-layer incompressible systems.

COMPARISON OF RESULTS WITH FIELD DATA

Attempts were made to compare the results shown in Figures 6 and 7 with earlier field test results. Field test results obtained by the Road Research Laboratory, England, are shown in Figure 8. Materials comprising the test road section are shown at the upper right corner. These studies indicated that the measured subgrade stresses decreased as the vehicle speed was increased from creep speed to about 15 mph; speeds above 15 mph remained constant. The curves from Figure 7 for τ_2 values between 1 and 10 have similar shapes as those obtained by the Road Research Laboratory. In both cases, the stresses decreased as the speed of the load increased and remained constant for v greater than 15 mph. For τ_2 greater than 10, the stress vs speed curves were nearly horizontal straight lines, indicating that the stresses were independent of the speed. It was beyond the scope of this study to determine experimentally the appropriate values of retardation times for various paving materials. However, it seems that a Kelvin model could be used for predicting the variation of vertical soil stresses for normal vehicle speeds, provided the values of G_{12}, τ_{12}, and τ_2 are properly determined.

The speed-deflection data obtained from the AASHO Road Test (23, p. 104) show that the deflection decreased almost linearly with increasing vehicle speed. Results of the present study also show (Fig. 6) that the displacement decreased with increasing vehicle speed, but the variation was not linear. Moreover, the computed rate of decrease of displacement with increasing vehicle speed was faster than that observed in the AASHO Road Test. However, this difference does not invalidate the results obtained in this study, because the displacements computed herein assumed incompressibility of materials and were for a point 2 ft below the surface, while the data obtained in the AASHO tests were taken on the

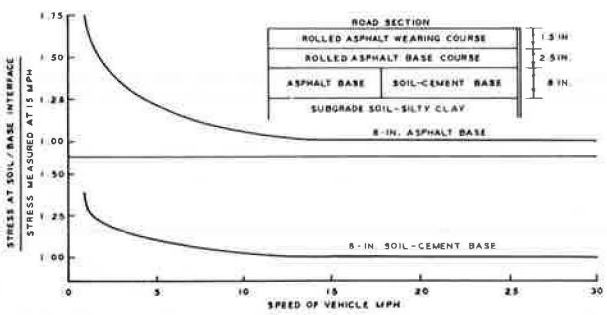

Figure 8. Test results from Road Research Laboratory, England.

surface and under actual road conditions. It is believed that a model with more elements than the Kelvin model, and the consideration of compressibility of the material may yield better results.

Although the numerical examples presented herein bear no direct relation to the field tests conducted earlier, it strongly indicates that solution capability is available for this class of problems. It is reasonable to assume that an appropriate model can be designed to represent a given pavement structure, using the method of computation in this paper and laboratory data of stress and displacement as functions of time and speed. Values of the model's parameters may be determined by using the method suggested by Schapery (24), which employs a collocation method for fitting the response of finite element viscoelastic models to experimental data over the entire time scale.

CONCLUSIONS

The objective of this research was to make an analytical study of the response of materials in highway pavement systems to moving traffic loads. Equations were developed for stresses and displacements at any point in an incompressible, viscoelastic pavement induced by a moving point load. The equations were then analyzed numerically on a high-speed digital computer for various types of materials at different speeds of the moving load. The major conclusions resulting from the analyses are as follows:

1. Because of the time-dependent nature of the material in the viscoelastic pavement, the solutions for stresses and displacements were also time-dependent. The stress and displacements depended upon the magnitude and speed of the load, the elastic and viscous components of the shear response of the material, the ratios of retardation time in layered systems, and time.
2. The time-dependent response of the material resulted in retardation of stress and displacement due to a moving load. The interaction between speed and material properties produced continued displacement for a short time after the load moved away from the station.
3. In all cases, the stress and displacement decreased with increasing speed of the load as well as with increasing value of retardation time of the material.
4. For two-layer systems, the maximum stress always occurred when the load was directly over the station, and the stress was compression. When the load moved toward or away from the station, the stresses possibly changed signs. The stress decreased with increasing speed of the load, and then reached a constant value as the speed exceeded 15 mph.
5. For two-layer systems, the displacements at the bottom layer were reduced due to an overlying reinforcing layer. The displacements were further reduced by increasing the retardation time of the reinforcing layer. The effect of the reinforcing layer, however, decreased with increasing speed of the moving load and with increasing value of the retardation time of the bottom layer.
6. The general shapes of the curves in single- and two-layer systems were similar. It is believed that the shapes of curves in systems with a greater number of layers and more complex materials would also be similar to those of single- and two-layer systems.
7. The theory of linear viscoelasticity qualitatively describes the material behavior under moving loads better than under stationary loads because of the relatively smaller stresses and displacements under a moving load.

ACKNOWLEDGMENT

Thanks are due the late Dr. Tilton E. Shelburne, State Highway Research Engineer, and J. H. Dillard, Head of the Bituminous Section, Virginia Highway Research Council; and C. N. Gaylord, Head and Professor of Civil Engineering, University of Virginia, for the assistance and encouragement in the conduct of the study.

The authors gratefully acknowledge the interest and financial support provided by the U. S. Bureau of Public Roads which made this study possible.

REFERENCES

1. Pister, K. S., and Monismith, C. L. Analysis of Flexible Viscoelastic Pavements. HRB Bull. 269, p. 1-15, 1960.
2. Pagen, C. A. Rheological Response of Bituminous Concrete. Highway Research Record 67, p. 1-26, 1964.
3. Monismith, C. L., and Secor, K. W. Viscoelastic Behavior of Asphalt Concrete Pavements. International Conference on the Structural Design of Asphalt Pavements, 1962.
4. Williams, M. L., Blatz, P. J., and Schapery, R. A. Fundamental Studies Relating to Systems Analysis of Solid Propellants. Galcit 101, Guggenheim Aeronautical Laboratory, California Institute of Technology, Feb. 1961.
5. Williams, M. L. Structural Analysis of Viscoelastic Materials. ATTA Jour., Vol. 2, p. 785-808, May 1964.
6. Lee, E. H. Stress Analysis in Viscoelastic Bodies. Quarterly of Applied Mathematics, Vol. 13, p. 183-190, 1955.
7. Pister, K. S. Viscoelastic Plate on a Viscoelastic Foundation. Jour. Engineering Mechanics Div., ASCE, Vol. 87, p. 43-54, Feb. 1961.
8. Ishihara, K. The General Theory of Stresses and Displacements in Two-Layer Viscoelastic Systems. Soils and Foundation (Japan), Vol. 2, p. 51-67, 1962.
9. Westmann, R. A. Viscoelastic and Thermoelastic Analysis of Layered Systems. Ph.D. dissertation, University of California, 1962.
10. Pister, K. S., and Westmann, R. A. Analysis of Viscoelastic Pavements Subjected to Moving Loads. International Conf. on Structural Design of Asphalt Pavements, 1962.
11. Westmann, R. A. Viscoelastic Layered System Subjected to Moving Loads. Jour. Engineering Mechanics Div., ASCE, June 1967.
12. Thompson, W. E. Analysis of Dynamic Behavior of Roads Subject to Longitudinally Moving Loads. Highway Research Record 39, p. 1-24, 1963.
13. Perloff, W. E., and Moavenzadeh, E. Deflection of Viscoelastic Medium Due to a Moving Load. International Conf. on Structural Design of Asphalt Pavements, 1967.
14. Timoshenko, S., and Goodier, J. N. Theory of Elasticity. McGraw-Hill, 1951.
15. Burmister, D. M. The General Theory of Stresses and Displacements in Layered Soil Systems. Jour. of Applied Physics, Vol. 16, p. 89-94, 126-127, 296-302, 1945.
16. Mehta, M. R., and Veletsos, A. S. Stresses and Displacements in Layered Systems. Civil Engineering Studies, Structural Research Series No. 178, University of Illinois, 1959.
17. Chou, Y. T. Stresses and Displacements in Viscoelastic Pavement Systems Under a Moving Load. Ph.D. thesis, University of Virginia, 1968.
18. Thomson, W. T. Laplace Transformation. Prentice-Hall, 1950.
19. Titchmarsh, E. C. The Theory of Functions. Oxford University Press, 1939.
20. Schapery, R. A. Approximate Methods of Transform Inversion for Viscoelastic Stress Analysis. Proc. 4th U. S. National Congress of Applied Mechanics, p. 1075-1085, 1962.
21. Huang, Y. H. Stresses and Displacements in Viscoelastic Layered Systems Under Circular Loaded Areas. International Conf. on Structural Design of Asphalt Pavements, 1967.
22. Whiffin, A. C., and Lister, N. W. The Application of Elastic Theory to Flexible Pavements. International Conf. on Structural Design of Asphalt Pavements, 1962.
23. Highway Research Board. AASHO Road Test Report 5—Pavement Research. Special Report 61E, 1962.
24. Schapery, R. A. A Simple Collocation Method for Fitting Viscoelastic Models to Experimental Data. California Institute of Technology, Nov. 1961.

The Analysis of a Homogeneous, Cross-Anisotropic Elastic Half Space Undergoing Deformations That Possess a Vertical Plane of Symmetry

C. M. GERRARD, C.S.I.R.O., Division of Soil Mechanics, Australia

This paper contains solutions for displacement, strain, and stress components produced throughout a homogeneous, cross-anisotropic elastic half space by loadings of a particular class. This class includes only loadings that are distributed over a circular area, and that give rise to a deformation field that has a vertical plane of symmetry. The loading conditions considered are unidirectional horizontal shear stresses, a linear variation in vertical direct stress, and a linear variation in vertical displacement.

•THE presence of patterns of structural anisotropy in soils is likely to be widespread and the reasons for this have been discussed previously (6). With this in mind a homogeneous, cross-anisotropic, elastic half space has been chosen as a simple model of earth masses because it possesses the symmetries that often exist in the structures of such masses. (A cross-anisotropic elastic body has an "η" fold axis of symmetry or an axis of symmetry of rotation passing through each of its points; hence, its properties in all directions perpendicular to that axis are identical but different to the properties parallel to the axis.) The number of elastic parameters involved with this material is five instead of two as for an isotropic material.

In this paper the class of deformations of a homogeneous, cross-anisotropic half space that have a vertical plane of symmetry are investigated. Three loading systems are considered (Fig. 1). The loads are applied over circular areas and are described briefly in the following.

•Loading Condition A—A uniform distribution of unidirectional horizontal shear stresses. Loading of this type produces a resultant horizontal thrust and is therefore typical of the braking and traction loads imposed on road pavements and horizontal loads developed in foundations due to the action of wind.

•Loading Condition B—A linear variation of vertical direct stresses. In this case the diameter along which the steepest gradient of vertical direct stress occurs is at right angles to the diameter along which the vertical direct stresses are zero. Since this type of loading develops a resultant moment but no resultant vertical force, it can therefore be used to analyze the action of moments on foundations.

•Loading Condition C—A linear variation of vertical displacement. This is analogous to loading condition B although the vertical displacement is defined rather than the vertical direct stress. Again there is a resultant moment but no resultant vertical force. Also the diameter along which the steepest gradient of vertical displacement occurs is at right angles to the diameter along which the vertical displacements are zero.

Half the loaded areas for both loading conditions B and C are required to withstand vertical tensile stresses. Such a requirement could be rarely met in practical soil mechanics and hence the main value of solutions for these conditions is when they are

Paper sponsored by Committee on Mechanics of Earth Masses and Layered Systems.

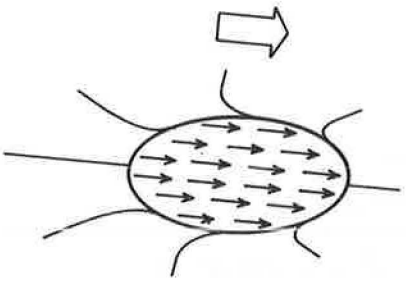

A. Unidirectional horizontal shear stresses

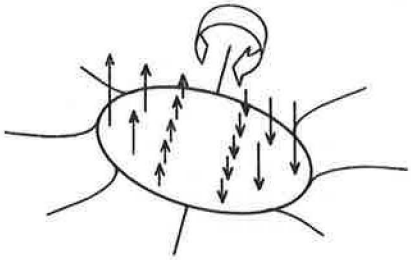

B. Linear variation in vertical direct stress

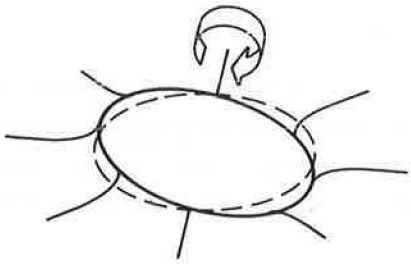

C. Linear variation in vertical displacement

Figure 1. Loading conditions.

used in conjunction with solutions for a loading condition where there is a resultant vertical force of sufficient magnitude to prevent the development of vertical tensile stresses in the foundation. Two such loading conditions have been considered previously by Gerrard (6), who has given solutions for a total of five axisymmetric loadings applied to a homogeneous, cross-anisotropic elastic half space. These loadings are: (a) uniform vertical direct stress, (b) uniform vertical displacement, (c) linearly increasing radial shear stresses, (d) linearly increasing torsional shear stresses, and (e) linearly increasing torsional shear displacement.

Thus, it can be readily seen that a range of complex loading systems, applied over circular areas, can be analyzed by superimposing the solutions for these axisymmetric loading conditions onto the solutions for the three loading conditions considered in this paper.

The aim in providing these latter solutions has been to evaluate all displacement, strain and stress components at all points throughout the half space. The reason for this is that the most critically loaded zones from a soil mechanics point of view may not necessarily lie on the load axis. In addition it is often necessary to be able to estimate the total fields of any or all of the stresses and/or strains and/or displacements when assessing the behavior of loaded earth mass.

Loadings of a similar nature to those discussed in this paper have been previously considered by Barber (1, 2), Muki (8), and Westmann (13, 14). However, all of this work is restricted to isotropic materials and in addition the solutions presented are not as comprehensive as those given here.

However, the stresses produced in a cross-anisotropic half-plane by loadings in the form of either a vertically or horizontally acting line load have been calculated by De Urena et al (4). In a further paper (9), these workers have integrated the above results to produce solutions for the cases of triangular distributions of vertical and horizontal loading stresses acting over a finite width. The respective resultant external loadings required in these cases would be (a) a combined moment and vertical thrust, and (b) a horizontal thrust. Thus these loading conditions are analogous to some of the loadings over circular areas considered in this paper and the previous work (6).

NOTATION

General

r, θ, z — cylindrical coordinates

u, v, w — displacements in corresponding coordinate directions

$\widehat{rr}$, $\widehat{\theta\theta}$, $\widehat{zz}$, $\widehat{rz}$, $\widehat{\theta z}$, $\widehat{r\theta}$ — direct stress and shear stress components of the stress tensor

$\epsilon_{rr}, \epsilon_{\theta\theta}, \epsilon_{zz}$
$\epsilon_{rz}, \epsilon_{\theta z}, \epsilon_{r\theta}$ — direct strain and shear strain components of the strain tensor

a, b, c, d, f — components of the elasticity tensor

E_H — modulus of elasticity in the horizontal direction

E_V — modulus of elasticity in the vertical direction

ν_H — Poisson's ratio—effect of horizontal strain on complementary horizontal strain

ν_{HV} — Poisson's ratio—effect of horizontal strain on vertical strain

ν_{VH} — Poisson's ratio—effect of vertical strain on horizontal strain

E — modulus of elasticity—isotropic material

ν — Poisson's ratio—isotropic material

Quantities and Parameters Involved in Solutions

$$\alpha^2 = \frac{ad - c^2 - cf + f(ad)^{1/2}}{2fd}$$

$$\beta^2 = \frac{ad - c^2 - cf - f(ad)^{1/2}}{2fd}$$

$$\gamma^2 = \frac{a - b}{f}$$

δ = maximum vertical displacement (inches)

$$\sigma = \arcsin\left\{\frac{2}{\left[\psi^2 + (1 + r)^2\right]^{1/2} + \left[\psi^2 + (1 - r)^2\right]^{1/2}}\right\}$$

$$\lambda = \arctan\left(\frac{2\psi}{\psi^2 + r^2 - 1}\right)$$

$$\phi = \alpha - \beta$$

$$\rho = \alpha + \beta$$

$$\ell_1 = \frac{d\alpha^2 - \frac{f}{2}}{\left(c + \frac{f}{2}\right)\alpha}$$

$$\ell_2 = \frac{d\alpha^2 + \frac{f}{2}}{\left(c + \frac{f}{2}\right)\alpha^2}$$

$$m_1 = \frac{\left(c + \frac{f}{2}\right)\left(\alpha^2 - \beta^2\right)}{f\beta} = \frac{\left(c + \frac{f}{2}\right)\rho\phi}{\frac{f}{2}(\rho - \phi)}$$

$$m_2 = \frac{\left(c + \frac{f}{2}\right)}{\frac{f}{2}} \cdot \frac{\alpha^2}{c + d\alpha^2}$$

$$m_3 = -\frac{2^{1/2}}{\pi^{1/2}} \cdot \frac{(c + d\rho^2)(c + d\phi^2)}{d(\rho^2 - \phi^2)}$$

$$m_4 = -\frac{2^{1/2}}{\pi^{1/2}} \cdot \frac{c + d\alpha^2}{2d\alpha}$$

$$\eta = \left[(\psi^2 + r^2 - 1)^2 + 4\psi^2\right]^{1/4}$$

p = maximum vertical loading pressure (psi)

$$q_1 = \frac{d\phi^2 - \frac{f}{2}}{\left(c + \frac{f}{2}\right)\phi}$$

$$q_2 = \frac{d\rho^2 - \frac{f}{2}}{\left(c + \frac{f}{2}\right)\rho}$$

r = horizontal offest from load axis/r_0 (inch/inch)
r_0 = loaded radius (inches)
s = unidirectional horizontal shear stress (uniform distribution) (psi)
z = depth from surface/r_0 (inch/inch)

STRESS-STRAIN RELATIONSHIPS

For a cross-anisotropic elastic material the stresses can be expressed in terms of the strains by:

$$\widehat{rr} = a\,\epsilon_{rr} + b\,\epsilon_{\theta\theta} + c\,\epsilon_{zz} \tag{1a}$$

$$\widehat{\theta\theta} = b\,\epsilon_{rr} + a\,\epsilon_{\theta\theta} + c\,\epsilon_{zz} \tag{1b}$$

$$\widehat{zz} = c\,\epsilon_{rr} + c\,\epsilon_{\theta\theta} + d\,\epsilon_{zz} \tag{1c}$$

$$\widehat{r\theta} = (a - b)\,\epsilon_{r\theta} \tag{1d}$$

$$\widehat{rz} = f\,\epsilon_{rz} \tag{1e}$$

$$\widehat{\theta z} = f\,\epsilon_{\theta z} \tag{1f}$$

The relations expressing the direct strains in terms of the direct stresses together with others expressing the elasticity components a, b, c, d in terms of the Young's moduli and Poisson's ratios have been given previously (6).

The strain components are

$$\epsilon_{rr} = \frac{\partial u}{\partial r} \tag{2a}$$

$$\epsilon_{\theta\theta} = \frac{u}{r} + \frac{1}{r} \cdot \frac{\partial v}{\partial \theta} \tag{2b}$$

$$\epsilon_{zz} = \frac{\partial w}{\partial z} \tag{2c}$$

$$2\,\epsilon_{rz} = \frac{\partial u}{\partial z} + \frac{\partial w}{\partial r} \tag{2d}$$

$$2\epsilon_{\theta z} = \frac{\partial v}{\partial z} + \frac{1}{r} \cdot \frac{\partial w}{\partial \theta} \tag{2e}$$

$$2\epsilon_{r\theta} = \frac{1}{r} \cdot \frac{\partial u}{\partial \theta} + \frac{\partial v}{\partial r} - \frac{v}{r} \tag{2f}$$

METHOD OF SOLUTION AND PRESENTATION OF RESULTS

The method of solution of problems involving the static loading of layers of cross-anisotropic elastic material, previously outlined by Gerrard and Mulholland (7), is based on the integral transform techniques developed by Sneddon (10) and Tranter (11). The problem considered in this paper, i.e., a homogeneous half space undergoing deformations that possess a vertical plane of symmetry, is a special case of the general range of problems that may be solved by this method.

For all three loading conditions the solutions for the displacements, strains, and stresses involve integrals of products of Bessel functions. In order to simplify presentation, these integrals have been abbreviated according to the following notation:

$$I(\eta, \tau, \chi, \psi) = \int_0^\infty J_\eta(k) \cdot J_\tau(kr) \cdot k^\chi \cdot e^{-\psi k} \cdot dk \tag{3a}$$

$$J(\eta, \tau \pm \mu, \chi, \psi) = \int_0^\infty J_\eta(k) \left[\frac{J_\tau(kr) \pm J_\mu(kr)}{2}\right] \cdot k^\chi \cdot e^{-\psi k} \cdot dk \tag{3b}$$

The form of solution obtained for the types of deformation considered has been shown to depend on the parameters α^2 and β^2 that are functions only of the elastic constants (7). Hence, for each of the loading conditions, three complete lists of solutions are given for the following cases:

1. Cross-anisotropic, α^2 positive, β^2 positive;
2. Cross-anisotropic, α^2 positive, β^2 zero;
3. Isotropic; this is a particular case of item (2) with $\alpha^2 = 1$, $\beta^2 = 0$.

Appended to the solutions for each loading condition is a section dealing with the evaluation of the relevant integrals. These sections are divided into three parts depending upon whether the integrals are to be evaluated:

1. At a general point within the system (i.e., $r \neq 0$, $\psi \neq 0$);
2. At a point on the load axis ($r = 0$); or
3. At a point on the surface ($\psi = z = 0$).

With regard to the evaluation of the integrals at a general point it can be seen from the lists that simple and direct results are obtained for loading condition C where the surface displacements are defined. However, this is not so for the defined stress conditions (A and B) where the integrals had to be evaluated by numerical integration, on a high-speed digital computer, for a range of values of r and ψ.* Some of these integrals have been previously tabulated by Eason, Noble, and Sneddon (5) for different ranges of values of r and ψ than were used in the current work. For anisotropic materials the parameter ψ is in the form of either ρz, ϕz, αz, or γz and therefore is a function of both the elastic parameters and the depth. This means that when using the tables* to calculate the stresses, strains, and displacements at a particular point within the system it will be generally necessary to interpolate between the tabulated points along the ψ coordinate.

*The tabulated values of a total of 22 such integrals are in Tables 1 through 22, which are included in a lengthy Appendix not published in this Record, but which is available from the Highway Research Board at the cost of reproduction and handling. Refer to XS-24, Highway Research Record 282.

At points on the load axis (i.e., $r = 0$) the integrals involved in all of the loading conditions can be evaluated simply and directly. On the other hand for points on the surface (i.e., $\psi = z = 0$) the integrals for all loading conditions become discontinuous in nature, in order to fulfill the loading conditions. As indicated most of the integrals have simple results while the remainder yield results in the form of hypergeometric functions (10, 12). Integrals whose coefficients contain z' have not been considered since their products (z·I or z·J) are in general zero for points on the surface. The values of integrals given in this paper are based directly or indirectly on the results obtained by Watson (12), Sneddon (10) and Bateman Manuscript Project (3).

In all solutions the orientation reference in any horizontal plane is given by $\theta = 0$ or π along the direction of the vertical plane of symmetry in the displacement patterns.

TOTAL MOMENT-DEFINED DISPLACEMENT RELATIONSHIP

For loading condition C it is possible to derive relationships between the defined surface displacement and the requisite applied moment. These relationships, found by integrating the moment of the vertical direct stress over the loaded area, are as follows:

Cross-anisotropic: α^2 positive, β^2 positive

$$\text{Total moment} = -\frac{8}{3} \cdot \delta \cdot r_o \cdot \frac{(c + d\rho^2)(c + d\phi^2)}{d(\rho + \phi)\rho\phi} \cdot \frac{\frac{f}{2}}{c + \frac{f}{2}} \tag{4a}$$

Cross-anisotropic: α^2 positive, β^2 zero

$$\text{Total moment} = -\frac{8}{3} \cdot \delta \cdot r_o \cdot \frac{(c + d\alpha^2)^2}{2\,d\alpha^3} \cdot \frac{\frac{f}{2}}{c + \frac{f}{2}} \tag{4b}$$

Isotropic

$$\text{Total moment} = -\frac{8}{3} \cdot \delta \cdot r_o \cdot \frac{E}{2(1 - \nu^2)} \tag{4c}$$

ACKNOWLEDGMENTS

The work presented in this paper was carried out in the Department of Civil Engineering, University of Melbourne, under the direction of Professor A.J. Francis and Dr. J.R. Morgan. As such, it forms part of a total project sponsored by the Australian Road Research Board. The author wishes to thank Mr. W. Flower of the Computation Department, University of Melbourne, for his work in compiling the tables.

REFERENCES

1. Barber, E. S. Shear Loads on Pavements. Public Roads, Vol. 32, No. 6, 1963.
2. Barber, E. S. Shear Loads on Pavements. Public Roads Vol. 33, No. 8, 1965.
3. Bateman Manuscript Project. Tables of Integral Transforms. McGraw-Hill, 1954.
4. DeUrena, R., Piquer, J. S., Muzas, F., and Sanz Saracho, J. M. Stress Distribution in Cross-Anisotropic Media. Proc. 1st Cong. Int. Soc. Rock Mech., Lisbon, Vol. 1, p. 313-317, 1966.
5. Eason, G., Noble, B., and Sneddon, I. N. On Certain Integrals of the Lipschitz-Hankel Type Involving Products of Bessel Functions. Phil. Trans., Series A, Royal Soc. London, Vol. 247, p. 529-551, 1955.
6. Gerrard, C. M. The Axisymmetric Deformation of a Homogeneous, Cross-Anisotropic Elastic Half Space. Highway Research Record 223, p. 36-44, 1968.
7. Gerrard, C. M., and Mulholland, P. Hexagonally Anisotropic Layered Elastic Systems. Submitted to ASCE (Eng. Mech. Div.), 1967.

8. Muki, R. Asymmetric Problems of the Theory of Elasticity for a Semi-Infinite Solid and a Thick Plate. Progress in Solid Mechanics, Vol. 1, North Holland Pub. Co., Amsterdam, 1960.
9. Piquer, J. S., Muzas, F., De Urena, R., and Grajera, F. Foundations in Cross-Anisotropic Ground. Proc. 1st Cong. Int. Soc. Rock Mech., Lisbon, Vol. 1, p. 531-536, 1966.
10. Sneddon, I. N. Fourier Transforms. McGraw-Hill, 1951.
11. Tranter, C. J. Integral Transforms in Mathematical Physics. Methvens Monographs on Physical Subjects, 3rd Ed., 1966.
12. Watson, G. N. The Theory of Bessel Functions. 2nd Ed., Cambridge Univ. Press, 1944.
13. Westmann, R. A. Layered Systems Subjected to Asymmetric Surface Shears. Proc. Roy. Soc., Edinburgh, Vol. LXVI, Series A, Part 3, p. 140, 1963.
14. Westmann, R. A. Layered Systems Subjected to Surface Shears. Proc., ASCE, Eng. Mech. Div., Vol. 89, No. 6, p. 177, 1963.

Bearing Capacity of Purely Cohesive Soils With a Nonhomogeneous Strength Distribution

CLARENCE H. C. JAMES, Howard University;
RAYMOND J. KRIZEK, The Technological Institute, Northwestern University; and
WALLACE H. BAKER, Soil Testing Española, S.A., Madrid, Spain

Based on published evidence, an empirical rule is postulated to describe the nonhomogeneous distribution of undrained shear strength with depth for a purely cohesive soil. With the use of this rule, the associated soil bearing capacity for a strip load of uniform intensity is determined for a variety of nonhomogeneous strength distributions, and the results are presented in a series of charts and an equation. For such soils, the bearing capacity is found to be strongly dependent on the width of the applied load, and to a lesser extent on the degree of overconsolidation of the upper zone. In most cases, bearing capacity values determined on the basis of the postulated strength distribution rule do not differ significantly from values obtained by a conventional analysis in which an "average" shear strength is assumed constant with depth; however, the proposed method affords greater reliability. It is felt that the results obtained can be reasonably extrapolated to loaded areas of different shapes.

•MOST currently used bearing capacity analyses employ the assumption that the soil is homogeneous with respect to its characteristic strength parameters. Although this is an entirely reasonable assumption in many cases, there are other situations where it is decidedly in error. In this work, a study is made of the effect of a nonhomogeneous strength distribution with depth on the bearing capacity of purely cohesive soils. Based on a postulated empirical strength distribution rule, the bearing capacity is determined by a minimization process applied to the equilibrium equation.

ASSUMPTIONS

The following assumptions are employed in this study:

1. A $\phi = 0$ analysis is valid, and potential failure surfaces are cylindrical in shape.
2. The nonhomogeneous in situ undrained shear strength distribution with depth obeys an empirical relation subsequently postulated.
3. The soil is isotropic with respect to its shear strength.
4. The applied surface load is of uniform intensity.

STRENGTH DISTRIBUTION WITH DEPTH

Published Evidence

The evidence gleaned over the years from examination of boring logs has led investigators to subscribe to the hypothesis that, in general, the in situ undrained shear strength, c_u, of a normally consolidated clay increases linearly with depth or with the

Paper sponsored by Committee on Mechanics of Earth Masses and Layered Systems and presented at the 48th Annual Meeting.

vertical effective normal stress, p, of the overburden; specifically, the shear strength ratio, c_u/p, is a constant. The undrained shear strength is usually determined by one or more of the following methods: (a) unconfined compression tests; (b) undrained triaxial tests on undisturbed samples at unaltered water content; (c) direct shear tests; or (d) directly in the field by vane shear tests.

Skempton (1, 2) attempted to correlate c_u/p with the plasticity index, I_P, and the liquid limit, w_L, of the soil, and he showed that some relation with I_P seemed to exist for normally consolidated marine clays. This latter correlation has proved to be convenient because it has been confirmed by sufficient field evidence to allow natural shear strengths of marine clays to be estimated for preliminary design purposes on the basis of simple laboratory tests. The Skempton relationship, discussed also by Terzaghi and Peck (3), is expressed as

$$\frac{c_u}{p} = 0.11 + 0.0037\, I_P \qquad (1)$$

However, even for marine clays, caution should be exercised in the use of this relation because, as data published by Feyling-Hanssen (4) show, there may be large deviations from values given by Eq. 1, particularly when considering the effects of leaching.

Feyling-Hanssen (4) published an exhaustive study of the relationship of micropaleontology to the shear strength characteristics of Norwegian marine clays, and he showed that, on the basis of their content of the fossil Foraminifera, it is possible to divide some normally consolidated Norwegian marine clays into stratigraphic zones (strata). Since, in clays of similar mineral composition and grain size distribution, a close correlation exists between a given stratigraphic zone and the shear strength, any one stratigraphic zone can be related to a particular value of c_u/p. In many cases the clay in any one stratigraphic zone exhibits a greater c_u/p value in deposits near sea level than in deposits situated at a greater elevation; this phenomenon demonstrates the general relationship between the geotechnical properties of a clay mass and the reduced salt concentration in the porewater of the clay. Small values of c_u/p occur in relatively salt-free clays, whereas high c_u/p values are found in clays which have, more or less, retained their original salt concentration.

Wu (5) examined soil samples from four areas of the Great Lakes region of North America. These lakes were formed as a result of the activities of continental glaciers during Pleistocene times and a number of soft clay deposits extending to great depths are known to exist in areas formerly occupied by glacial lakes. Wu measured the shear strength of these clays by unconfined compression tests and by undrained triaxial tests and, at all sites, he found that there was a general tendency for the strength to increase with depth within each individual stratum. In some cases, relatively high strengths near the surface reflect the effect of overconsolidation. These results also showed that the overall trend is one of increasing c_u/p ratio with increasing values for the plasticity index; furthermore, the higher the sensitivity and the liquid limit of the clays, the lower was the c_u/p value. These latter clays exhibited a flocculent or honeycomb structure which is normally associated with random particle arrangement.

Kenney (6) further points out that, since the c_u/p ratio of clays is dependent on the clay fabric, the effective stress strength parameters, the history of the clay, and the method by which the shear strength is determined, it is strongly dependent upon the geological history of the soil. He contends that, because the magnitude of the Skempton (7) pore pressure coefficient, A, for a certain type of test reflects the rigidity and the resilience of the soil structure, and because these properties are dependent on the method of deposition of the soil particles and the nature of any subsequent physiochemical changes in these particles, A, and therefore c_u/p, is probably chiefly dependent upon the geologic history of the clay. Since I_P depends on the results of two empirical tests (the liquid limit and plastic limit tests), both of which are conducted on completely remolded soil, it is difficult to visualize a relationship that is generally reliable and, at the same time, as simple as Eq. 1.

Hansen (8) introduced the following expression for the in situ shear strength of a clay mass:

$$c_u = c_1 + \alpha_1 \gamma z \tag{2}$$

where c_1 and α_1 are soil parameters that must be determined empirically; α_1, which ranges in value between 0 and 0.3, is a function of the coefficient of earth pressure at rest, a "cohesion factor," the effective angle of internal friction, and a factor, λ, introduced by Skempton (9). Given the value of α_1, c_1 is chosen such that c_u will express the approximate vane strengths (or one-half the undrained compressive strengths) at different depths.

Empirical Strength Distribution Rule

Since the in situ undrained shear strength of a clay is often a function of depth, it is reasonable to postulate a simple, empirical strength distribution rule which contains soil parameters, which may be determined from standard laboratory tests, and empirical coefficients, which will insure a goodness of fit for the strength data from a given soil profile. Accordingly (Fig. 1), the total undrained shear strength, c_t, at a point located a vertical distance, z, below the ground surface may be expressed as

$$c_t(z) = c_o + (c_u/p)\gamma_b z + F\, c_o \exp\left[-(z/\alpha b)^n\right] \tag{3}$$

where γ_b is the submerged unit weight of the soil, c_o is the zero intercept on the strength axis of the linear portion of the composite strength curve, and F, α, and n are empirical coefficients, which are discussed subsequently. The empirical coefficients are dimensionless, and the other parameters must be expressed in a consistent set of units.

Over the years, the findings of many investigators have shown that, for normally consolidated and slightly overconsolidated clays, the most probable range of values for c_u/p is from 0 to 0.3, and these findings have been satisfactorily substantiated in this study through calculations of c_u/p from soil profiles and laboratory or field data found in the literature. The last term on the right-hand side of Eq. 3 reflects the condition of greater shear strength in the upper few feet of the clay as a result of overconsolidation due to dessication or fluctuation of the groundwater table. The role of F is to establish a maximum value for c_t at the upper surface of the overconsolidated zone; it is unreasonable to assume too high a value for F because a high degree of overconsolidation at the surface would probably cause surface cracks and preclude the existence of any strength in this region. From an examination of many soil profiles, it has been concluded that the most probable range for values of F is 0 to 2, with a maximum of 4. The coefficient α describes the attenuation rate of the effect of this assumed overconsolidation in the upper zone; for this study, values of α are assumed to range from 0.025 to 0.4. Practical estimates for α can be obtained by choosing the z/b value at which the strength difference between the curve describing the data and the extended straight-line portion of that curve is approximately equal to one-third of $F\, c_o$. The exponential coefficient n describes the manner in which the strength due to the assumed overconsolidation in the upper zone

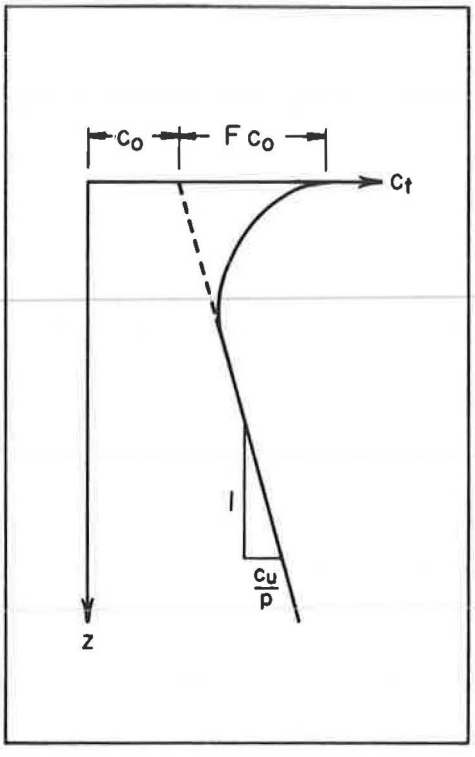

Figure 1. Assumed strength distribution with depth.

$$\exp\left[-\left(\frac{z}{ab}\right)^n\right]$$

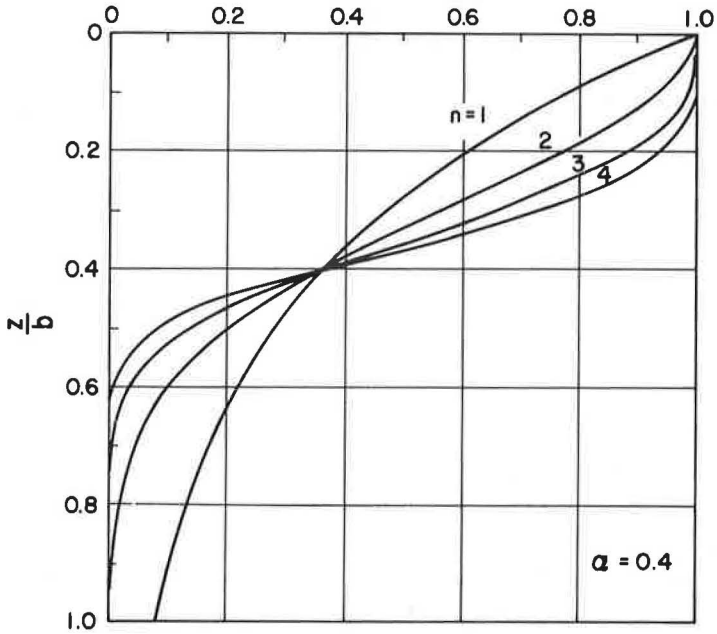

Figure 2. Effect of n on nature of strength variation in upper zone.

varies with depth. Typical variations for n = 1, 2, 3, and 4 are shown in Figure 2; however, a value of one was used in this work. Finally, a range of 500 to 4000 psf was chosen for c_o, and the total weight density was assumed to be 100 pcf.

The proposed strength distribution rule is general enough to include cases where the undrained shear strength is constant, increases, or decreases with depth. If c_u/p equals zero, the bearing capacity analysis will be similar to the conventional one, except that full consideration will be given to any condition of overconsolidation in the upper zone. When c_u/p and F both vanish, c_t equals c_o, which, in turn, equals the conventional constant cohesion parameter, c, for a homogeneous soil, and the procedure degenerates to a conventional $\phi = 0$ analysis. Difficulties in applying the postulated strength distribution rule in subsequent calculations are encountered when c_o vanishes; one practical way to avoid this problem is to decrease the slope, c_u/p, slightly so that c_o becomes greater than zero. However, in real soils the probability of c_o being equal to or less than zero is very small.

DETERMINATION OF BEARING CAPACITY

For a strip load of width, 2 b, applied to the surface of a purely cohesive soil whose undrained strength characteristics are represented by Eq. 3, the bearing capacity, q, based on the assumption of a cylindrical failure surface, can be determined by utilizing a minimization procedure in conjunction with the equilibrium equation. Figure 3 shows a typical failure surface for such a problem as stated above; although Meyerhof (10) cautioned that ". . . where the subsoil is neither homogeneous nor isotropic . . . the error . . . will increase with increasing inhomogeneity. . . ," the assumption of a cylindrical failure surface is justified on the bases that (a) it closely agrees with the Prandtl surface for the $\phi = 0$ case, (b) it has the advantage of simplicity from a computational standpoint, (c) it leads to bearing capacity values which are in general agreement with values calculated by more sophisticated methods, and (d) the effect of resulting

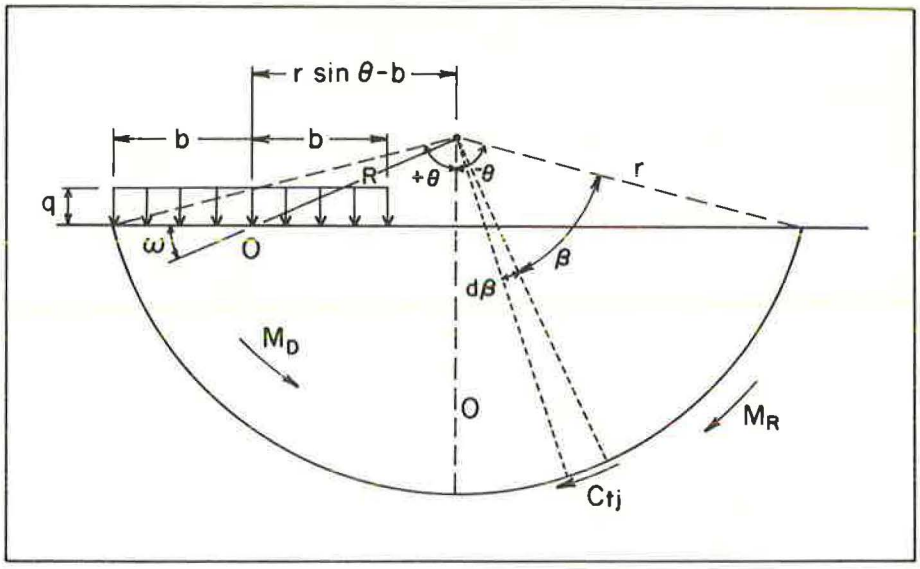

Figure 3. Assumed failure mechanism and notation.

inaccuracies is reduced because bearing capacity ratios or differences are considered. Two advantages of this assumption are that body forces are eliminated from the equilibrium equation and that the geometry is simple.

Equilibrium conditions dictate that the driving moment, M_D, must equal the resisting moment, M_R. Because of symmetry, the body forces cancel, and the driving moment is produced only by the load, while the resisting moment is developed by the shear strength of the soil along the potential failure surface. Referring to the geometry in Figure 3, we may write the equilibrium equation as

$$q\ (2\,b)(r\ \sin\theta - b) = r^2 \int_{-\theta}^{\theta} c_t\ d\beta \tag{4}$$

where c_t may be considered, in general, a function of r and β. If the arc length from $-\theta$ to θ is divided into m equal angular increments, $\Delta\beta$, and if the shear strength, c_t, is assumed to be a constant value, c_{tj}, over each increment of arc length, $r\,\Delta\beta$, Eq. 4 may be approximated by

$$q\ (2\,b)(r\ \sin\theta - b) = r^2 \sum_{1}^{m} c_{tj}\,\Delta\beta = 2\,r^2(\theta/m) \sum_{1}^{m} c_{tj} \tag{5}$$

which, when solved for q, becomes

$$q = \frac{r^2\theta}{b^2 m}\ \frac{1}{\frac{r\ \sin\theta}{b} - 1} \sum_{1}^{m} c_{tj} \tag{6}$$

Since c_{tj} is a function of r and β, q, as given by Eq. 6, is not a function merely of two variables, r and θ; hence, its evaluation cannot be made by the procedure of setting equal to zero the derivatives of the function with respect to r and θ, and finding the

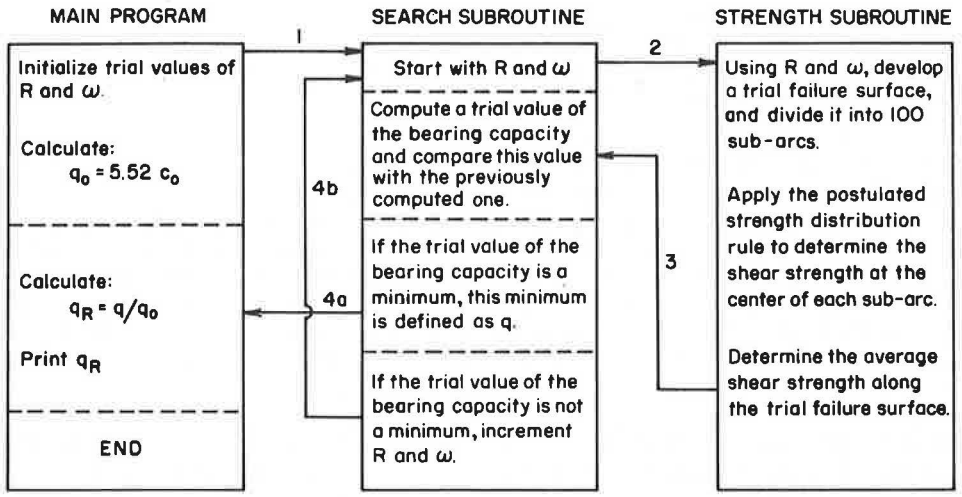

Figure 4. Flow diagram of computer procedures.

unique combination of r and θ that minimizes q. Instead, the function q is minimized by applying a modified version of the Direct Search technique discussed by Katz et al (11), Hooke and Jeeves (12), and Wilde (13).

In order to provide a basis for comparison of this bearing capacity with the more conventional bearing capacity determined by multiplying an "average" cohesion, c, by a bearing capacity factor, N_c, we assume that F and c_u/p are zero; hence, c equals c_o, and N_c equals 5.52. According to Taylor (14), this value of 5.52 for N_c is the same as that given by Fellenius for the case of a cohesive soil in which shear strength is independent of spatial coordinates; it can be derived analytically by solving Eq. 6 with c_{tj} equal to a constant, c, and defining N_c as q/c. If we differentiate N_c with respect to θ and with respect to r, and set each derivative equal to zero, simultaneous solution of the resulting two equations gives a relation between r and θ from which N_c can be evaluated. If q_c is defined as a reference bearing capacity value, given by

$$q_c = c_o N_c \tag{7}$$

we can define a dimensionless bearing capacity ratio, q_R, such that

$$q_R = q/q_c \tag{8}$$

Equation 8 gives the relation between the bearing capacity determined from the postulated strength distribution rule given by Eq. 3 and the bearing capacity determined by assuming a constant "average" cohesion given by c_o.

COMPUTER PROGRAM

Figure 4 is a flow diagram of the procedures followed in determining the bearing capacity as described herein.

Main Program

Choose as the initial values for r and θ those critical values which are associated with the conventional bearing capacity; the initial value of θ is approximately 66.6 deg; and the radius, r, is a function of θ and the half-width, b, of the proposed load. Instead of using r and θ as the independent variables, however, we choose R and ω; these variables are shown in Figure 3, and they have the advantage that the origin, O, remains fixed.

Subroutines for Modified Direct Search

From trigonometric relationships between r, R, θ, and ω, determine starting values of R and ω, and proceed as follows:

1. Enter the strength subroutine and select a trial failure surface.
2. Divide this trial failure surface arc into 100 sub-arcs and, by means of Eq. 3, determine the shear strength at the center of each sub-arc.
3. Determine the average shear strength along the entire trial failure surface.
4. Reenter the search subroutine and use Eq. 6 to compute the first trial value of q.
5. Sequentially increment R and ω in an exploratory move to establish the appropriate direction so that the new value of q will be less than or equal to the preceding value. If a positive increment does not produce the desired result, a negative increment is tried; if neither alternative succeeds, the variable is left unchanged and attention shifts to the next variable. Once the exploratory moves have established a direction, a pattern move is begun; this pattern move involves an increment which is the vector sum of the two preceding successful R and ω increments. If the pattern move is successful, the pattern step is doubled for the next move. If, during a pattern move, q increases beyond the preceding value, we retreat to the previous "base point" and initiate an exploratory move to build a new pattern. If this, too, is a failure, the magnitude of the increment is decreased and an attempt is made at a new exploratory move. The search terminates when the increment sizes fall below minimum values of R/8000 and ω/8000, or when the magnitude of the difference between the latest trial value of q and the preceding value is less than a minimum which was set at 0.001 times the preceding value of q. This minimum trial value is the bearing capacity q.
6. Return to the main program and compute q_R.

RESULTS

The soil bearing capacity was determined for applied load widths, 2 b, of 5, 10, 20, 40, 80, and 160 ft; for each case, the soil strength distribution was varied, the variations being reflected in different values of c_o (500, 1000, 2000, and 4000 psf), c_u/p (0, 0.1, 0.2, and 0.3), α (0.025, 0.1 and 0.4), and F (0, 1, and 4). Hence, bearing capacity values for 1,152 different cases were computed. Since it is not feasible to present individual results for each of these 1,152 cases, the following approximation has been developed.

For given values of c_o, c_u/p, and α, the difference between the bearing capacity for F equal to 0 and that for F equal to any other value up to 4 is approximately proportional to the value of F, that is,

$$q - q_0 \cong MF \tag{9}$$

where q_0 can be determined from the bearing capacity ratios, q_R, given in Figure 5, and M is a proportionality coefficient which, based on calculations for a variety of cases, is reasonably independent of c_o, c_u/p, and b, and can be approximated by

$$M \cong 0.2\,\alpha\,q_0 \tag{10}$$

As indicated by the combination of Eqs. 7 and 8, q, and in particular q_o, can be expressed as

$$q_0 = q_R\,q_c = q_R\,c_o\,N_c = 5.52\,q_R\,c_o \tag{11}$$

Finally, substitution of Eqs. 10 and 11 into Eq. 9 yields

$$q \cong 5.52\,q_R\,c_o\,(1 + 0.2\,\alpha\,F) \tag{12}$$

For the ranges of variables considered herein, it has been verified that Eq. 12 predicts to within about 2 percent the bearing capacity determined by the more sophisticated

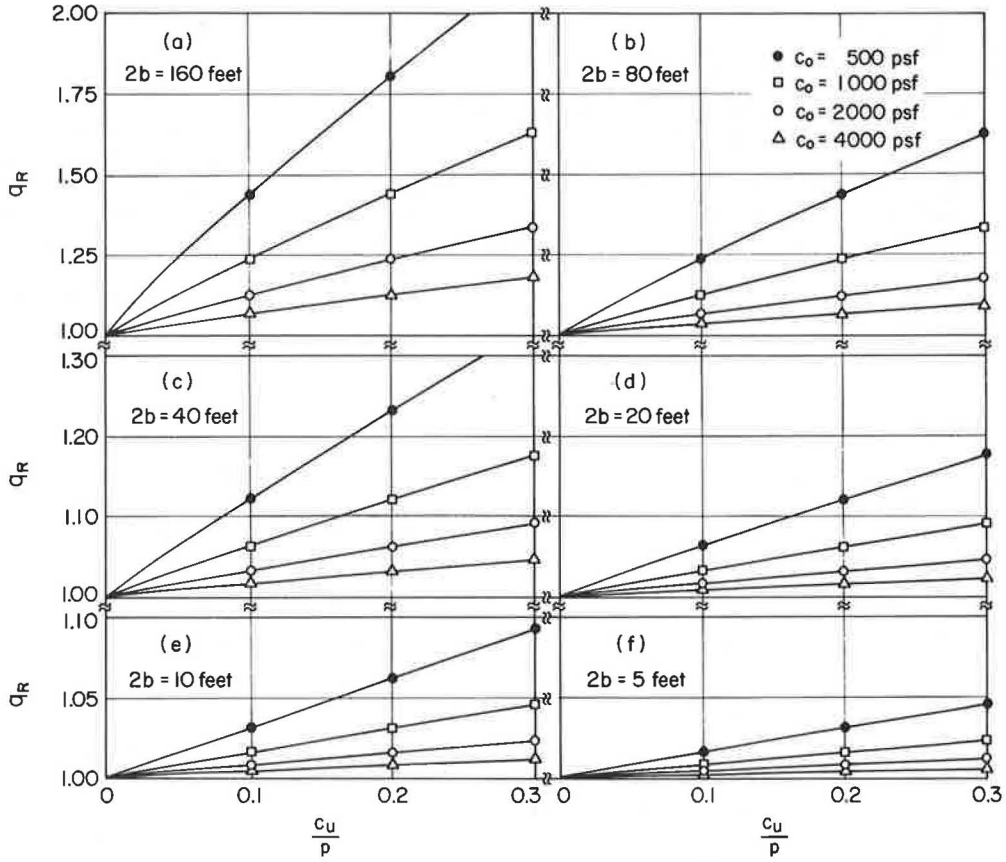

Figure 5. Bearing capacity ratios for F = 0.

procedure previously described. However, additional work has indicated that the bearing capacity determined by the use of an "average" shear strength that is constant with depth does not result in values significantly different from those obtained by this procedure.

The use of these results to determine the bearing capacity of a purely cohesive soil with a nonhomogeneous strength distribution of the type shown in Figure 1 may be explained as follows. The width of the load must be known, and c_o, c_u/p, α, and F (n is assumed equal to 1) must be estimated from a knowledge of the particular soil deposit under consideration or by describing laboratory or field test data with a curve similar to that shown in Figure 1. With a knowledge of 2 b, c_o, and c_u/p, a value for q_R is obtained from Figure 5; this value for q_R, together with the values for c_o, α, and F, is then substituted in Eq. 12 to determine the bearing capacity, q.

CONCLUSIONS

Based on a limited study of the bearing capacity of nonhomogeneous, purely cohesive soils subjected to a surface strip load of uniform intensity, the following conclusions may be drawn.

1. A reasonable approximation (within about 2 percent) of the soil bearing capacity under the conditions described can be simply and quickly obtained from a knowledge of the width of the loaded area and an estimate of the parameters describing the strength distribution with depth in the soil. Although the specific results herein were determined

for a strip load, it seems entirely reasonable that these results can be extrapolated with little error to other shapes of loaded area.

2. Use of a more sophisticated, empirical, undrained shear strength distribution rule, as opposed to the use of an "average" shear strength that is constant with depth, does not result in significantly different values for bearing capacity. However, an advantage of the proposed strength distribution rule is the increased degree of confidence it provides by representing more realistically the actual strength distribution in the field, and bearing capacity values determined on the basis of this rule should be more reliable than those resulting from the assumption of an "average" undrained shear strength.

3. The bearing capacity is found to be strongly dependent on the width of the applied load, and to a lesser extent on the effect of overconsolidation in the upper zone.

REFERENCES

1. Skempton, A. W. Vane Tests in the Alluvial Plain of the River Forth Near Grangemouth. Geotechnique, Vol. 1, No. 2, p. 111-124, London, 1948.
2. Skempton, A. W. Discussion on The Planning and Design of the New Hong Kong Airport. Proc. Institution of Civil Engineers, Vol. 7, p. 305-307, London, 1957.
3. Terzaghi, K., and Peck, R. B. Soil Mechanics in Engineering Practice. 2nd Ed., John Wiley, p. 117, 1968.
4. Feyling-Hanssen, R. Micropaleontology Applied to Soil Mechanics in Norway. Norwegian Geotechnical Institute, Pub. No. 20, 1957.
5. Wu, T. Geotechnical Properties of Glacial Lake Clays. Trans. ASCE, Vol. 125, p. 994-1012, 1960.
6. Kenney, T. C. Discussion of Geotechnical Properties of Glacial Lake Clays. Trans. ASCE, Vol. 125, p. 1012-1021, 1960.
7. Skempton, A. W. The Pore-Pressure Coefficients A and B. Geotechnique, Vol. 4, No. 4, p. 143-147, London, 1954.
8. Hansen, B. A General Plasticity Theory for Clay. Geotechnique, Vol. 3, No. 4, p. 154-164, London, 1952.
9. Skempton, A. W. A Study of the Immediate Triaxial Test on Cohesive Soils. Proc. Second International Conf. on Soil Mechanics and Foundation Engineering, Rotterdam, Vol. 1, p. 192-196, 1948.
10. Meyerhof, G. G. Discussion on Bearing Capacity of Footings on Layered Clays. Jour. Soil Mechanics and Foundations Div., ASCE, Vol. 93, No. SM5, Part I, p. 361-363, 1967.
11. Katz, D. L., Carnahan, B., Douty, R. T., Hauser, N., McMahon, E. L., Zimmerman, J. R., and Seider, W. D. Computers in Engineering Design Education. Vol. 1, Summary Report, p. 54-63, 1966, Univ. of Michigan.
12. Hooke, R., and Jeeves, T. A. Direct Search Solution of Numerical and Statistical Problems. Jour. Assoc. for Computational Machines, Vol. 8, No. 2, p. 212-229, 1962.
13. Wilde, D. J. Optimum Seeking Methods. Prentice-Hall, Chap. 3, 1964.
14. Taylor, D. W. Fundamentals of Soil Mechanics. John Wiley, p. 573-575, 1948.

Effectiveness of Leaky Sheetpile

RAYMOND J. KRIZEK, The Technological Institute, Northwestern University; and
GABOR M. KARADI, University of Wisconsin—Milwaukee

The steady-state seepage flow under and through a leaky sheetpile partially embedded in a homogeneous, isotropic porous medium underlain by an impervious substratum is studied by means of its electric analog. Results are correlated with limited cases of previous theoretical and experimental work, and they are extended to include the cases of a partially embedded sheetpile centered under an impervious dam, and a single sheetpile, either fully or partially penetrating a porous stratum with horizontal potential boundaries. The effectiveness of a sheetpile is shown to decrease markedly with a very small percentage of holes in the sheetpile, and charts are given to evaluate quantitatively the extent of this decrease.

•MOST classical solutions for seepage flow around a sheetpile contain the very restrictive assumption that the sheetpile is completely impervious. Although this assumption is desirable to render the problem tractable, it is not satisfied in most practical engineering situations. Usually the sheetpile is not 100 percent impervious over its entire depth, but rather it contains a random distribution of leaks due to open seams between the pilings, distortions in the piling caused by driving, etc. This work is directed toward evaluating quantitatively the effectiveness of such a leaky sheetpile for both the fully penetrating and partially penetrating cases.

SCOPE OF STUDY

This study is restricted to steady-state seepage flow under and through a vertical leaky sheetpile embedded in a homogeneous porous medium underlain by an impervious substratum. The variables under study are shown in Figure 1, and they include the quantity of flow per unit time, q; the head difference between the potential boundaries, h; the coefficient of permeability of the porous medium, k; the thickness of the porous medium (or depth to the impervious substratum), D; the depth of penetration of the sheetpile, d; the open space in the sheetpile, W; and the half-width of the impervious dam, b. Since the above six variables are expressed in terms of two fundamental units (e.g., length and time), four dimensionless terms may be formed to describe the results; these are chosen for this study as the flow quantity parameter, q/kh, penetration parameter, d/D, open-space ratio, W/d, and dam width parameter, b/D.

NATURE OF STUDY

This study is experimental in nature and utilizes the well-known electrical analog technique (1). The porous medium of permeability k is modeled geometrically by a conductive paper (Teledotos paper) with electrical conductivity C (which equals the reciprocal of the resistivity, R); the hydraulic potential difference, h, is analogous to the electrical voltage difference, V, while the fluid flow quantity, q, is represented by the electrical current flow, I. Hence, we have the equivalence

$$\frac{q}{kh} = \frac{I}{CV} = N \qquad (1)$$

Paper sponsored by Committee on Foundations of Bridges and Other Structures.

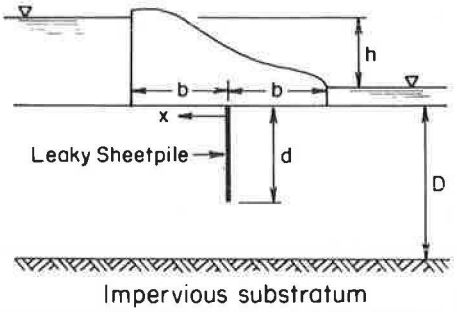

Figure 1. Diagrammatic description of problem.

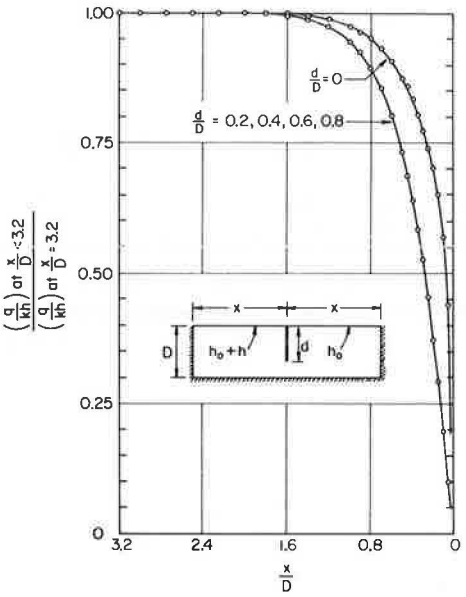

Figure 2. Effect of unnatural boundaries.

where N is a geometric shape factor which is constant for similar geometric shapes and analogous boundary conditions.

Since the geometrical conditions under study are symmetrical about the vertical sheetpile, all analog results presented herein were obtained with models representing one-half the geometrical configuration shown in Figure 1. For reasons which will become apparent later, all models were constructed with a depth, D, of 12.5 in. In order to eliminate or minimize the effect of unnatural boundary conditions on the models, a study was made of the influence of the parameter x/D on q/kh for five values of d/D (0, 0.2, 0.4, 0.6, 0.8) with b/D and W/d equal to zero. These results (Fig. 2) indicate that the effect of the unnatural boundary conditions at either end is negligible for x/D values greater than 2; a very conservative x/D value of 4 was used for all tests conducted in this investigation. A slight anisotropy of about 8 to 10 percent between the principal conductivities of the Teledotos paper was noted. To partly neutralize this effect, the "reference square," which was used to complete one leg of the Wheatstone bridge, was cut at 45 deg to the longitudinal axis of the paper, and all models were cut from the roll with consistent orientations, but otherwise the effect of this anisotropy was ignored.

All of the leaky sheetpiles treated herein were modeled by a series of equally spaced slits. A completely ineffective sheetpile (W/d = 1.00) is, of course, modeled by a conductive strip of constant potential. The open-space ratio, W/d, of the sheetpile is decreased by arbitrarily dividing the sheetpile depth, d, into 1.25-in. increments and punching a series of equally spaced 0.125-in. square holes, one in each 1.25-in. increment, along the length of the sheetpile; this having been completed, the sheetpile is considered to have a W/d ratio of 0.90, and appropriate readings are recorded. Then, another 0.125-in. square hole is punched from each 1.25-in. increment, yielding W/d equal to 0.80, and appropriate readings are again taken. This process is repeated with the refinement that for W/d values less than 0.30, the ratio is decreased in increments of 0.05 instead of 0.10.

REVIEW OF THEORETICAL SOLUTIONS

A slit model, similar to that previously described, was used in the analytical approach reported by Dachler (2, 3), who derived

$$E = \frac{\ln \sin \frac{\pi W}{2D}}{\ln \sin \frac{\pi W}{2D} - \frac{n\pi b}{2D}} \qquad (2)$$

where n is the number of openings and E is an effectiveness or efficiency factor defined as

$$E = \frac{q_o - q}{q_o} \tag{3}$$

where q_o is the flow which would occur under an impervious dam with a width ratio of b/D and no sheetpile; the flow quantities q and q_o are both determined for the same head difference, h, across the potential boundaries. Note, however, that Eq. 2 is applicable only to the case of a fully penetrating sheetpile (d/D = 1.0), since the open-space ratio is expressed as W/D rather than W/d; also, it is restricted to the case where the sheetpile is centrally located under a dam of width ratio b/D, since E erroneously becomes unity if b/D equals zero. For W/D values less than 0.10, Eq. 2 can be simplified within slide-rule accuracy to

$$E = \frac{\log_{10} \frac{2D}{\pi W}}{\log_{10} \frac{2D}{\pi W} + \frac{n\,b}{1.465\,D}} \tag{4}$$

As can be seen from Eqs. 2 and 4, for constant values of W/D and b/D, an increase in n has the effect of lowering E; this effect is not at all intuitively obvious and it appears somewhat paradoxical.

A theoretical approach to the solution of the leaky sheetpile problem for conditions of horizontal free-field flow was presented by Numerow (4); his work is based on the assumption that the stream function, ψ, is distributed linearly along the sheetpile according to

$$\psi = \frac{\alpha\, qy}{D} \tag{5}$$

where y is the vertical coordinate and α is a dimensionless parameter characterizing the permeability or leakiness of the sheetpile. Using a particular method of solution developed by him, Numerow obtained the following simple relationship to express the effect of sheetpile leakiness:

$$f = \sigma f^{\infty} = \frac{\phi}{\phi + Df^{\infty}} f^{\infty} \tag{6}$$

where σ is a parameter which characterizes the effectiveness of the leaky sheetpile; f is the ratio of the permeability, k, of the porous medium times the additional head loss, Δh, caused by the sheetpile to the flow rate, q, for the leaky sheetpile, i.e., $f = (k\Delta h)/q$; f^{∞} is the value of f for a perfectly impermeable sheetpile; and ϕ, which characterizes in a manner similar to α the leakiness of the sheetpile (this latter parameter was introduced by Chugaew (5) and used subsequently by Numerow (4)), equals Df/α. The value of f^{∞} can be determined from

$$f^{\infty} = \frac{4}{\pi} \ln \tan^{-1} \frac{\pi}{4}\left(1 - \frac{d}{D}\right) \tag{7}$$

where d is the penetration of the sheetpile. Certain laboratory investigations (5) indicate that the value of ϕ, which has the dimension of length, lies between 5 and 80 m, but field measurements by different investigators indicate that the value of ϕ may be as high as 2000 m, with increasing values of ϕ corresponding to decreasing values of sheetpile leakiness. Based on the theoretical results of Numerow (4), Figure 3 is proposed to determine the effectiveness of a leaky sheetpile for different values of d/D and ϕ/D. Since ϕ is not directly related to the number of leaks in the sheetpile, the applicability

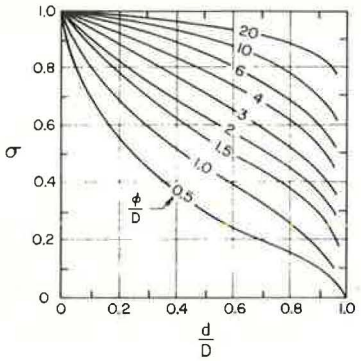

Figure 3. Theoretical effectiveness of a leaky sheetpile.

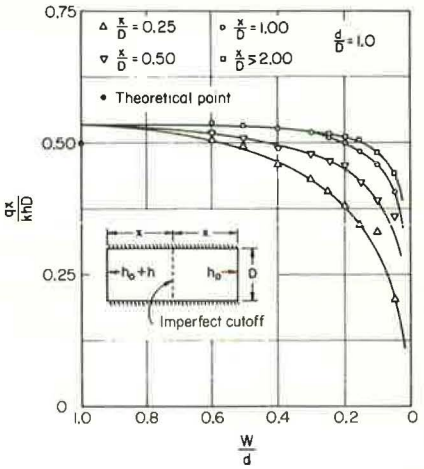

Figure 4. Effectiveness of an imperfect cutoff on one-dimensional flow quantity.

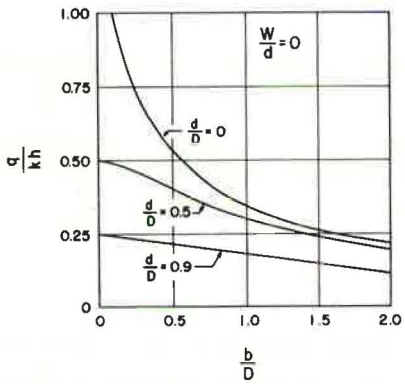

Figure 5. Theoretical relationship between flow parameter and width of dam.

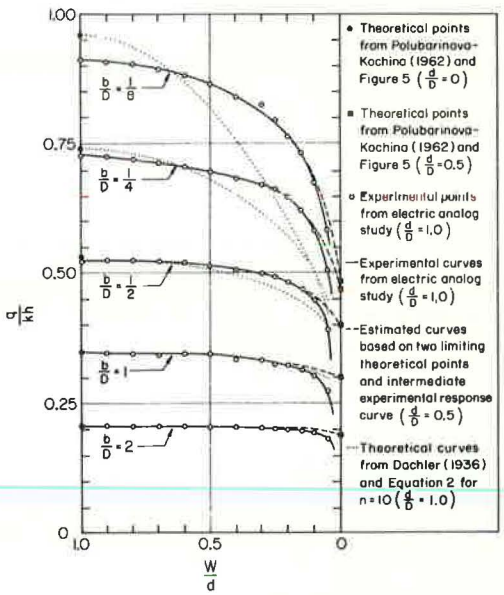

Figure 6. Effectiveness of a single sheetpile centered under a dam.

of α as a parameter characterizing the leakiness of the sheetpile may be viewed with some doubt.

EXPERIMENTAL RESULTS

By use of the experimental technique described, an initial study was conducted for the case of an imperfect cutoff (d/D = 1.0) intercepting horizontal flow, and the results are shown in Figure 4. The modified flow parameter, qx/khD, is used to obtain consistency in expressing the results. The deviation between the theoretical and experimental values (about 7 percent) at W/d equal to zero is attributed to the anisotropy of the conductive paper. Above an x/D value of 2.0, flow quantities were not significantly affected by variations in x/D.

By combining the results of model studies on a sheetpile centered under an impervious dam and the theoretical solutions presented by Polubarinova-Kochina (6) and Dachler (2), the information in Figures 5 and 6 is obtained. Figure 5 illustrates graphs of q/kh as a function of b/D for cases of no sheetpile (d/D = 0) and completely effective sheetpiles (W/d = 0) with depth ratios d/D, of 0.5 and 0.9; these theoretical curves,

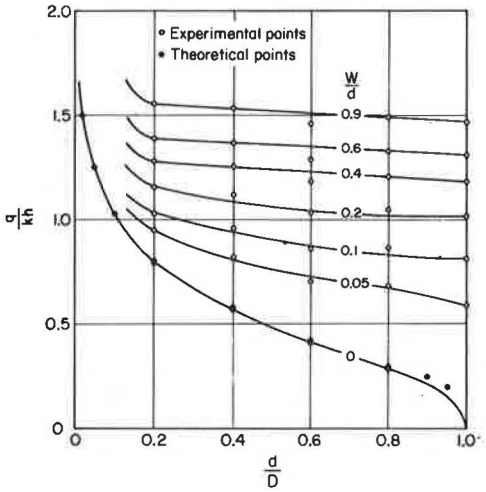

Figure 7. Effectiveness of an isolated leaky sheetpile.

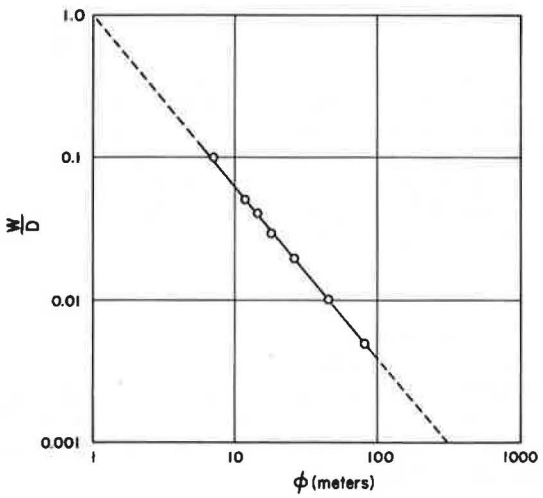

Figure 8. Experimental relationship between open-space ratio and permeability characteristic of a leaky sheetpile.

obtained from Polubarinova-Kochina (6), provide some limiting conditions for the experimental results in Figure 6. The open circles represent experimental data for the flow parameter q/kh associated with a fully penetrating (d/D = 1.0) sheetpile; the solid circles at the left of the graph represent theoretical calculations for the case where there is no sheetpile (d/D = 0 or W/d = 1). The solid squares at the right of the graph indicate theoretical results for a fully effective (W/d = 0) partially penetrating sheetpile where d/D equals 0.5, and the dashed curves represent estimates of the anticipated results for leaky sheetpiles with d/D equal to 0.5. Due to the apparent small differences in q/kh for partially and fully penetrating sheetpiles with W/d values greater than 0.05, it was not deemed necessary to conduct additional experiments for partially penetrating sheetpiles centered under dams; the indicated estimates appear to provide an adequate evaluation of such cases. As seen from Figure 6, as b/D increases, q/kh becomes less sensitive to W/d, except for very low values (less than 0.05); also, there appears to be very little difference between the seepage quantity under a completely effective sheetpile (W/d = 0) which penetrates the pervious layer halfway (d/D = 0.5) and a fully penetrating sheetpile (d/D = 1.0) for which W/d equals 0.05. The dotted curves (Fig. 6) were calculated by Eq. 2 with d/D equal to 1 and n equal to 10, the same condition which was achieved experimentally. Eq. 2 agrees very well with the experimental data for large values of b/D, but deviations in excess of 20 percent are noted for low values of b/D. As mentioned previously, Eq. 2 is not applicable to cases where b/D equals 0, that is, the case of a single isolated sheetpile.

The final case considered is that of a single sheetpile (b/D = 0) partially or fully penetrating the pervious layer. Since a singularity exists at the intersection of the sheetpile and the horizontal potential surfaces for the case where b/D equals 0, this singularity was eliminated experimentally by approximating the single sheetpile case by the case where b/D is equal to 0.01. The results obtained from an extensive series of analog model tests are shown in Figure 7; the data for the fully effective sheetpile case (W/d = 0) agree very closely with the theoretical solution of Polubarinova-Kochina (6).

In order to evaluate the ability of the more abstract parameter ϕ to characterize a leaky sheetpile in a manner similar to that accomplished by W/d, analog experiments were conducted with the sheetpile fully penetrating the permeable layer. In this case the value of f^{∞} is infinity, since a perfectly impermeable fully penetrating sheetpile does not allow any percolation through it, and from Eq. 6, we can write $f = \phi/D$ or $\phi = fD$; hence, the value of ϕ can be obtained as a function of W/D (d = D) directly from the experimental data. Figure 8 shows that, when plotted on a log-log scale, the obtained values of W/D and ϕ lie on a straight line which can be represented by

$$\frac{W}{D} = \phi^{-1.2} \tag{8}$$

where ϕ is expressed in meters. This relationship indicates that ϕ is, in fact, a parameter which characterizes the leakiness of the sheetpile. The laboratory experiments mentioned earlier (5) yielded ϕ values between 5 and 80 m, and these correspond to W/D values between 0.15 and 0.005; the high ϕ value of 2000 m obtained under field conditions corresponds to an extrapolated W/d value of 0.00011, which indicates an almost perfectly impermeable sheetpile.

CONCLUSIONS

Quantitative experimental relationships have been determined for the effectiveness of a leaky sheetpile which either partially or fully penetrates a homogeneous porous medium underlain by an impervious substratum; the sheetpile may be isolated or centered under an impervious dam. Based on the results of an electric analog investigation and correlation with limited theoretical work reported, the following conclusions can be advanced:

1. In virtually all practical cases the effectiveness of a sheetpile is reduced considerably by a relatively small open-space ratio in the sheetpile area.
2. The decrease in effectiveness is much more abrupt for fully penetrating sheetpiles centered under wide impervious dams than it is for isolated sheetpiles or those under narrow dams.
3. For low open-space ratios, the rate of decrease in effectiveness is considerably more rapid for a fully penetrating sheetpile than for a partially penetrating one.
4. For sheetpiles under wide impervious dams, there is relatively little difference in the seepage flow quantities under and through a leaky fully penetrating sheetpile and under and through a leaky partially penetrating sheetpile. In other words, the only way to effectively reduce the flow quantity is by installing a nearly impervious fully penetrating sheetpile.
5. For an isolated sheetpile with an open-space ratio greater than 0.1, there is little difference in the seepage flow quantity for a fully penetrating or partially penetrating sheetpile.
6. A relatively abstract parameter, proposed by other investigators to characterize the leakiness of a sheetpile, has been shown to correlate well with the more physical open-space ratio used in this study.

ACKNOWLEDGMENT

The conscientious and able assistance of Sidney Wagner, who conducted the experimental work reported herein, is gratefully appreciated.

REFERENCES

1. Cedergren, H. R. Seepage, Drainage, and Flow Nets. John Wiley, 1967.
2. Dachler, R. Grundwasserstromung. Springer, Vienna, p. 82, 1936.
3. Casagrande, A. Control of Seepage Through Foundations and Abutments of Dams. Geotechnique, Vol. 11, No. 3, p. 161-181, 1961.
4. Numerow, S. N. Consideration of the Permeability of Sheetpile for the Computation of Seepage Flow Under Concrete Dams. Inzhenernii Sbornik, Vol. 23, p. 164-172, 1956.
5. Chugaew, E. A. Seepage-Flow Calculations of a Hydraulic Structure Taking into Account the Permeability of the Sheetpiles. Proc., Federal Research Institute for Hydraulics, Vol. 48, p. 21-45, 1952.
6. Polubarinova-Kochina, P. Y. Theory of Ground Water Movement. Translated by J. M. R. DeWiest, Princeton Univ. Press, p. 91, 1962.